

**VIBRATION INDUCED STRESS AND ACCELERATED LIFE ANALYSES
OF AN AEROSPACE STRUCTURE**

**A THESIS SUBMITTED TO
THE GRADUATE SCHOOL OF NATURAL AND APPLIED SCIENCES
OF
MIDDLE EAST TECHNICAL UNIVERSITY**

BY

SERHAN ÖZSOY

**IN PARTIAL FULFILLMENT OF THE REQUIREMENTS
FOR
THE DEGREE OF MASTER OF SCIENCE
IN
MECHANICAL ENGINEERING**

JANUARY 2006

Approval of the Graduate School of Natural and Applied Sciences

Prof. Dr. Canan ÖZGEN
Director

I certify that this thesis satisfies all the requirements as a thesis for the degree of Master of Science.

Prof. Dr. Kemal İDER
Head of Department

This is to certify that we have read this thesis and that in our opinion it is fully adequate, in scope and quality, as a thesis for the degree of Master of Science.

Assoc. Prof. Dr. Mehmet ÇELİK
Co-Supervisor

Assoc. Prof. Dr. F. Suat KADIOĞLU
Supervisor

Examining Committee Members

Prof. Dr. Y. Samim ÜNLÜSOY (METU, ME) _____
Assoc. Prof. Dr. F. Suat KADIOĞLU (METU, ME) _____
Assoc. Prof. Dr. Mehmet ÇELİK (ASELSAN) _____
Prof. Dr. R. Orhan YILDIRIM (METU, ME) _____
Prof. Dr. Mehmet ÇALIŞKAN (METU, ME) _____

I hereby declare that all information in this document has been obtained and presented in accordance with academic rules and ethical conduct. I also declare that, as required by these rules and conduct, I have fully cited and referenced all material and results that are not original to this work.

Name, Last Name: Serhan ÖZSOY

Signature:

ABSTRACT

VIBRATION INDUCED STRESS AND ACCELERATED LIFE ANALYSES OF AN AEROSPACE STRUCTURE

ÖZSOY, Serhan

M.Sc., Department of Mechanical Engineering

Supervisor: Assoc. Prof. Dr. F. Suat KADIOĞLU

Co-Supervisor: Assoc. Prof. Dr. Mehmet ÇELİK

January 2006, 106 Pages

Fatigue failure of metallic structures operating under dynamic loading is a common occurrence in engineering applications. It is difficult to estimate the response of complicated systems analytically, due to structure's dynamic characteristics and varying loadings. Therefore, experimental, numerical or a combination of both methods are used for fatigue evaluations. Fatigue failure can occur on systems and platforms as well as components to be mounted on the platform.

In this thesis, a helicopter's Missile Warning Sensor - Cowling assembly is analyzed. Analytical, numerical and experimental approaches are used wherever necessary to perform stress and fatigue analyses. Operational flight tests are used for obtaining the loading history at the analyzed location by using sensors. Operational vibration profiles are created by synthesizing the data (LMS Mission Synthesis). Numerical fatigue analysis of the assembly is done for determining the natural modes and the critical locations on the assembly by using a finite element model (MSC Fatigue). In addition, numerical multiaxial PSD analysis is performed for relating the experimental results (Ansys). Residual stresses due to riveting are determined (MSC Marc) and included in experimental analysis as mean stresses. Bolt analysis is performed analytically (Hexagon) for keeping the

assembly stresses in safe levels while mounting the experimental prototype to the test fixture.

Fatigue tests for determining the accelerated life parameters are done by an electromagnetic shaker and stress data is collected. Afterwards, fatigue test is performed for determining whether the assembly satisfies the required operational life. Resonance test is performed at the frequency in which the critical location is at resonance, since there was no failure observed after fatigue testing. A failure is obtained during resonance test. At the end of the study, an analytical equation is brought up which relates accelerated life test durations with equivalent alternating stresses. Therefore, optimization of the accelerated life test duration can be done, especially in military applications, by avoiding the maximum stress level to reach or exceed the yield limit.

Keywords: Accelerated Life Testing, Exaggeration factor, Operational Flight Test, Experimental Stress Analysis.

ÖZ

BİR HAVACILIK YAPISINDA TİTREŞİM KAYNAKLI GERİLME VE HIZLANDIRILMIŞ ÖMÜR ANALİZLERİ

ÖZSOY, Serhan

Yüksek Lisans, Makine Mühendisliği Ana Bilim Dalı

Danışman: Doç. Dr. F. Suat KADIOĞLU

Eş-Danışman: Doç. Dr. Mehmet ÇELİK

Ocak 2006, 106 Sayfa

Dinamik yükler altında çalışan metalik yapılarda yorulma hasarlarına sıkılıkla rastlanmaktadır. Yapıların dinamik özellikleri ve değişken yüklerden dolayı sistemlerin tepkilerini analitik olarak tespit etmek zor olmaktadır. Bu nedenle, yorulma hesapları için deneysel yöntemler, sayısal metodlar veya her iki yöntem birlikte kullanılmaktadır. Yorulma hasarları, parçalarda oluşabildiği gibi entegre edildikleri sistem ve platformlarda da görülebilmektedir.

Bu tezde, helikopterlerin Füze İkaz Sensör (FİS) kaporta montajı çalışmaları analiz edilmiştir. Gerilme ve yorulma analizleri gerçekleştirilirken yerine göre analitik, sayısal ve deneysel yaklaşımlar kullanılmıştır. Bu kapsamında analizi gerçekleştirilen bölgeye ait yükleme tarihçesinin belirlenmesi amacıyla sistem monte edilecek bölgelere sensörler yerleştirilerek operasyonel uçuş testleri gerçekleştirilmiştir. Bu veriler sentezlenerek operasyonel titreşim profilleri oluşturulmuştur (LMS Mission Synthesis). Ayrıca montaj yapısının sonlu elemanlar modeli kullanılarak gerçekleştirilen sayısal yorulma analizleriyle (MSC Fatigue) rezonans salınım şekilleri ve kritik yorulma bölgeleri tespit edilmiştir. Bunların yanı sıra, bu çalışmaların deneySEL sonuçlarla bağlantısının kurulabilmesi amacıyla çok eksenli sayısal Güç Spektrum Yoğunluk analizi (Ansys) gerçekleştirilmiştir. Perçinleme kalıntı gerilmeleri sayısal analizle (MSC Marc)

elde edilmiş ve ortalama gerilme olarak deneysel analizlere dahil edilmiştir. Deneysel prototipin test fikstürüne montaj gerilmelerinin güvenli seviyelerde tutulabilmesi için analitik olarak civata analizi (Hexagon) gerçekleştirılmıştır.

Hızlandırılmış ömür parametrelerini bulmaya yönelik yorulma testleri birim zamanda elektromagnetik sarsıcı ile yapılmış ve bu esnada gerilme verileri kayıt edilmiştir. Daha sonra belirli bir hızlandırılmış yüklemeye yapının yeterli ömre sahip olup olmadığına anlaşılması için yorulma testleri gerçekleştirilmiştir. Proje için belirlenmiş ömürde hasar oluşmaması nedeniyle kritik noktanın salınım şekline göre belirlenmiş frekansta rezonans testi uygulanmış ve hasar gözlenmiştir. Çalışmanın sonunda hızlandırılmış test süreleri ile eşdeğer değişken gerilme genlikleri arasında bir eşitlik ortaya koyulmuştur. Böylelikle, özellikle askeri platformlarda gerçekleştirilecek olan hızlandırma ömür sürelerinin optimizasyonu en yüksek gerilme seviyesi akma limitini geçmeyecek şekilde yapılabilecektir.

Anahtar Kelimeler: Hızlandırılmış Ömür Testi, Yükseltme faktörü, Operasyonel Uçuş Testi, Deneysel Gerilme Analizi.

To My Family

ACKNOWLEDGEMENTS

I express my sincere appreciation to my thesis supervisor Assoc. Prof. Dr. Suat KADIOĞLU and co-supervisor Assoc. Prof. Dr. Mehmet ÇELİK for their supervision, support and helpful critics throughout the progress of my thesis study.

I would like to thank my friends Murat AYKAN and Fatma Serap AYKAN for their help.

The cooperation and friendly support of my colleagues in ASELSAN during my thesis study also deserves to be acknowledged.

Thanks to my parents and brother for their unique motivation and encouragement.

Finally, many thanks go to my fiancée Çiğdem NAMLI for her continuous help and understanding during my thesis study.

TABLE OF CONTENTS

PLAGIARISM.....	iii
ABSTRACT	iv
ÖZ	vi
ACKNOWLEDGEMENTS	ix
TABLE OF CONTENTS	x
LIST OF ABBREVIATIONS	xii
CHAPTER	
1. INTRODUCTION	1
1.1. Fatigue Phenomena	1
1.2. Accelerated Life Testing Concept.....	2
1.3. Overview of the Study	3
2. LITERATURE SURVEY	5
3. FATIGUE THEORY.....	10
3.1. Multiaxial Fatigue	11
3.2. Vibration Fatigue Approach	16
4. ACCELERATED LIFE TESTING.....	20
4.1. Frequency domain method.....	21
4.1.1. Frequency domain approaches in International Military Standards.....	24
4.2. Time domain method.....	26
5. OPERATIONAL FLIGHT TESTS AND MISSION SYNTHESIS	28
5.1. Operational Flight Tests and Data Acquisition.....	28
5.2. Mission Synthesis of Operational Data	34
6. NUMERICAL AND EXPERIMENTAL FATIGUE ANALYSIS OF MWS-COWLING ASSEMBLY	40
6.1. Numerical Fatigue Analysis of MWS-Cowling Assembly	40
6.2. Experimental Fatigue Analysis of MWS-Cowling Assembly	46
6.3. Failure Occurrence of MWS-Cowling Assembly by Resonance Tests.....	49
6.4. Comparison of Numerical and Experimental Fatigue Analysis Results	53

7. EXPERIMENTAL STRESS ANALYSIS OF THE ASSEMBLY BY ACCELERATED LIFE TESTING.....	55
7.1 Experimental Data Processes and Fatigue Stress Analysis	55
7.2. Obtaining Accelerated Life Testing Time Relation	63
8. DISCUSSION AND CONCLUSION.....	66
REFERENCES	69
APPENDICES	
A. EFFECT OF MEAN STRESS ON FATIGUE LIFE AND RAINFLOW CYCLE COUNTING METHOD	72
B. OPERATIONAL FLIGHT PROFILE.....	78
C. PRINCIPLES OF PIEZOELECTRIC SENSORS	79
D. BOLT ANALYSIS SHEET.....	81
E. MEASUREMENT UNCERTAINTY OF THE DATA.....	82
E.1 Gaussian or Normal Distributions	82
E.2. Random Error Estimation.....	87
E.3. Systematic or Bias Error Estimation.....	87
F. NUMERICAL PSD ANALYSIS OF THE ASSEMBLY.....	90
G. RIVETING SIMULATION FOR RESIDUAL STRESSES ON THE COWLING	95
H. STRAIN ROSETTE ANALYSIS THEORY	102
I. SKETCH OF THE ANALYZED LOCATIONS	105

LIST OF ABBREVIATIONS

- PSD: Power spectral density
MWS: Missile warning sensor
ALT: Accelerated life test
 a : Biaxiality ratio
 φ : Angle between and x-axis
 $\sigma_{1,2}$: Principal stresses
 σ_0 : von Mises stress
 ε_0 : Equivalent strain
 $H(f)$: Frequency response function
ICP: Integrated circuit piezoelectric
MRS: Maximum response spectrum
FDS: Fatigue damage spectrum
SDOF: Single degree of freedom
 f_n : Natural frequency of the SDOF system
 W : Amplitude of the vibration PSD
 t : Test duration
 Q : Damping of SDOF system
 b : Inverse slope of the Woehler curve
 n : Stress damping constant
 C_i : Number of cycles of individual stresses
 m : Averaging constant
 S_y : Yield strength of the material
 S_e : Fatigue strength of the material
 σ_a : Alternating stress
 σ_m : Mean stress
 c : Coefficient that relates equivalent stress with ALT duration
FA: Axial force
FQ: Transverse force

FK: Clamping load

FM: Initial clamping load

FV: Preload

FSA: Proportion of the axial load which additionally loads the bolt

FPA: Proportion of the axial load which unloads the clamped parts

tau: Torsional stress in threads

μ_G : General coefficient of friction

μ_K : Coefficient of friction for bolt head bearing surface

μ_{Tr} : Coefficient of friction for the interface

σ : Standard deviation

μ : Average of the population

E_{random} : Random error

E_{bias} : Bias error

N: Number of sub-records

RMS: Root mean square

$B_{effective}$: Effective bandwidth

$B_{halfpower}$: Half-power bandwidth

E: Young's modulus of the material

G: Shear modulus of the material

v: Poisson's ratio of the material

CHAPTER 1

INTRODUCTION

1.1. Fatigue Phenomena

Most of the engineering components and structures work under fluctuating or cyclic loads. Failure may occur in long term, although the level of the loading is not high enough to yield the structure immediately. Fatigue failure of materials is a function of repeated or variable loading. Therefore, fatigue analysis is essential to verify that the structures will be able to complete the required service period without any failure.

Fatigue damage is defined as the modification of the properties of a material, primarily due to formation of cracks resulting from cyclic loads that create oscillating stresses in the structure. It is a complicated process which is difficult to describe and analyze, even in microscopic scale [1]. A typical fatigue failure, in which a crack propagates and sudden failure occurs, is given in Figure 1.1. Zone marked with (A) indicates the fatigue crack growth and zone (B) indicates the eventual sudden fracture.

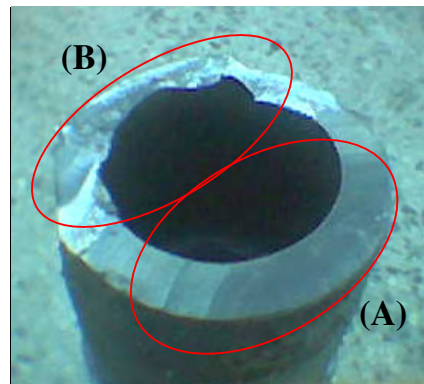


Figure 1.1: Fatigue failure location.

Fatigue performance of materials and structures are conceptual in behavior, like the mechanical strength characteristics. Consequently, fatigue performance tests of the structures should be performed individually to obtain a database that can be used in fatigue analyses.

1.2. Accelerated Life Testing Concept

Accelerated life testing (ALT) is a method of testing products and materials under amplified conditions which is employed at the early stage of development of products for saving testing time and cost. It has been used to obtain failure information within an acceptable time frame such that the life distribution of products and materials can be estimated at laboratory environment. Structures or systems are tested at high stress levels to cause possible early failures.

In many cases, the interest of the reliability analysis is in estimating distribution parameters under the standard operating conditions. This testing gives the information to predict the lifetime distribution under the simulated condition in a short time.

Mission Synthesis is an accelerated life test loading profile process in which fatigue equivalent model is evaluated for structures. It is basically used for obtaining standard and accelerated vibration profiles by using the actual test data. These profiles are usually preferred over the standards, since they represent the real life situations much better (Figure 1.2).

The mechanism behind mission synthesis process and the parameters used will be discussed in the following chapters.

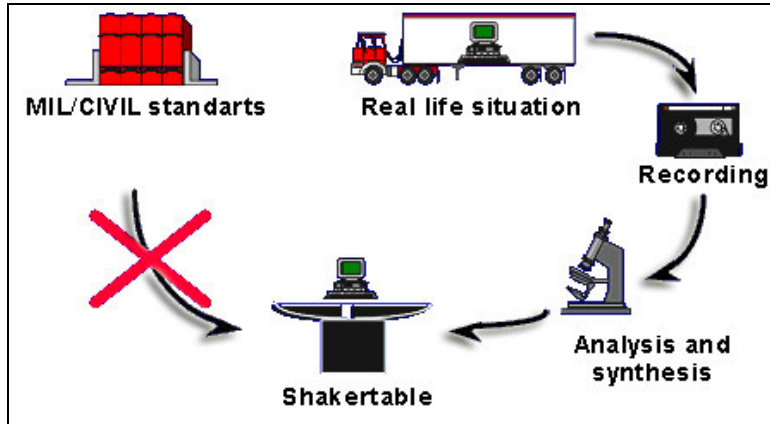


Figure 1.2: Mission Synthesis process flow chart [2].

1.3. Overview of the Study

In this study, the vibration induced stress and fatigue analysis of a helicopter component will be performed. The component, Missle Warning Sensor (MWS), is decided to be integrated on a helicopter's cowling. A typical application of MWS on a different helicopter is shown in Figure 1.3 and the physical MWS is shown in Figure 1.4.



Figure 1.3: An application of MWS on helicopters.



Figure 1.4: Missile Warning Sensor.

The function of MWS is to identify the missiles approaching the helicopter. It uses passive ultraviolet imaging sensors to detect, track and declare missile threats from information based on the plume emissions created by the propulsion system of the missile. Therefore, position of this equipment is very important to assure that maximum space around the helicopter is being scanned by the sensor. The solid model of MWS and cowling assembly is shown in Figure 1.5.

The fundamental loading for MWS and cowling assembly is the vibration due to helicopter operation. The fatigue analysis of the assembly under vibration loading needs to be performed. While performing the fatigue analysis in laboratory condition, Accelerated Life Testing approach will be used. Using the stress values obtained from the tests, a relation between stress and life acceleration period will be proposed. The details of these studies will be explained in the following chapters.

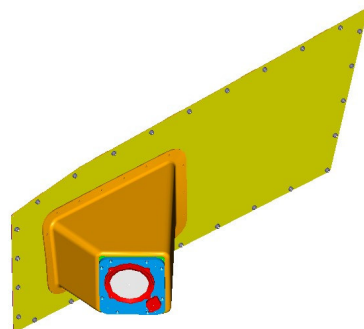


Figure 1.5: Solid model of MWS and cowling assembly.

CHAPTER 2

LITERATURE SURVEY

The fatigue problem under consideration in this study is a complex one due to the following factors:

- Cumulative damage under random loading containing different stress levels and different number of repetitions.
- Multiaxial stress state.
- Mean and residual stresses.
- Application of Accelerated Life Testing approach.

One or more, such issues have been addressed by many researchers in recent years. A brief review of some studies which are related to the work done in this study is given below.

Lagoda et al. [3] carried out a study to investigate the effect of mean stress on fatigue life of steel specimens. Experiments were performed under uniaxial random loading. Damage was calculated for cyclic stress histories with zero mean (symmetric) and cyclic stress histories with non zero mean (asymmetric) by using Rainflow Cycle Counting and Palmgren-Miner approach. It was found out that an appropriate amplitude transformation method should be applied on asymmetric histories in order to take the mean stress effect into account.

Szlowinski et al. [4] investigated the effects of the residual stress fields and squeeze forces applied during riveting process. The finite element analysis of a riveting process has been performed and the results were compared with experimental results. The effect of high residual stresses on the rivet and rivet holes for the fatigue life has been studied. Also the effect of rivet head and squeezing forces on fraying damage has been studied. According to the research, it has been found out that with high squeeze forces a zone of compressive

residual hoop stress dominated the area close to the hole, whereas a zone of tensile residual hoop stress was present on areas far from the hole. These stress fields were found out to be the major reason of the propagation of fatigue cracks at rivets/rivet holes.

Byrne et al. [5] proposed a technique to determine the multi axial fatigue damage for structures under complex loading. It uses the rainflow counting principle with von Mises equivalent stresses. Deviatoric stresses were obtained by stress filtering and used in order to simplify the procedure. Therefore, the method is appropriate for structures where failure criterion does not depend on hydrostatic stress. The outputs of this technique were compared with sample cases whose results are known. It was found out that the technique is practical to perform fatigue calculations of structures under complex multi axial loading.

Carpinteri et al. [6] carried out a study on expected principal stress directions under multiaxial loading. A theoretical procedure to calculate the Euler angles from the matrix of the principal direction cosines for a generic time instant was proposed. The procedure consists of averaging the instantaneous values of the three Euler angles through weight functions. It was examined how such theoretical principal directions determined by applying the proposed procedure are correlated to the position of the experimental fracture plane for some fatigue tests in the literature. The algorithm proposed is applied to some experimental biaxial in- and out-of-phase stress states to assess the correlation. From the results obtained, it was seen that in the case of a small phase angle, the normal vector to the experimental fracture plane agrees with the expected direction of the maximum principal stress.

Çelik [7] used experimental approach to perform the fatigue analysis of the launcher assembly of a military land vehicle. Finite element analysis was performed to determine the critical locations where strain rosettes were settled down on the physical prototype. Tests were carried out by performing operational life profile of the vehicle in the field. The proven ground is used to simulate harsh

environmental conditions with different cruise speeds of the tracked vehicle. Absolute maximum principal stresses were determined at each rosette location by analyzing the strain data collected. Rainflow Cycle Counting technique was applied with mission synthesis of operational profile on the stress data to determine equivalent mean and alternating stresses. Failure Criteria relations were used to convert these stresses to alternating stresses with zero mean. Fatigue life estimation of each location was obtained by using the equivalent stresses on S-N curve of the material.

Colombi et al. [8] compared two approaches used for fatigue estimation under random loading, namely, Rainflow Cycle (RFC) and Cycle Sequence (CSQ) models. In the study, the performance of the stochastic versions of these two methods were compared and applied to determine the fatigue lifetime of welded components. As a result, CSQ model gave better results since it includes the sequence effects due to its fracture mechanics formulation. It was also pointed out that, according to the numerical results obtained, non-Gaussian loading situation is more critical than Gaussian loading case having the same RMS level and the kurtosis on the same structure.

Winter et al. [9] developed a new approach for fatigue calculations which does not use Palmgren-Miner rule and apply cycle counting. The new model is capable of taking mean stress, frequency and threshold effects under wide band loading into account and it is called Damage Integral Model. J-integral is used to determine the stress and strain levels at the crack tip of a stationary or growing crack. Comparisons between the Damage Integral Model and several fatigue calculation methods were performed. It was found out that the model resulted similar to that of Rayleigh approximation under variable-amplitude (VA) loading. However, the model should be modified for cases under constant-amplitude (CA) loading.

Holm et al. [10] proposed a simple method to calculate the fatigue life of structures. The simple method was a combination of Palmgren-Miner rule with

time invariance. It is shown that these two approaches together fully simulate the real life situations. Exhaustion function was obtained by the damage caused due to periodically fluctuating loads. The function was used in the model to combine the damage caused by periodically fluctuating loads and a load varying in an arbitrary way. It was determined that the model is appropriate for fatigue life calculations of structures under periodically fluctuating loads.

Pitoiset et al. [11] developed a method in frequency domain to calculate the high-cycle fatigue damage for multiaxial stresses created by random vibrations. This approach is based on the definition of the von Mises stress as a uniaxial random process for which the PSD function is computed. It was shown that the approach can be generalized to include a frequency domain formulation of the multiaxial rainflow method for biaxial stress states. Similar results were obtained by applying these two methods individually and critical locations could be identified on the finite element model of the structure.

Fu et al. [12] investigated the fatigue failure of components having random stresses with bi-modal spectral densities. A new frequency domain method was devised for determining the probability density functions in the case of a spectral density with two peaks. The input spectral densities were determined by realistic simulation of vehicle suspensions. The results were compared with other frequency domain approaches and rainflow counting method in time domain. It was found out that the bi-modal method gave as accurate results as the time domain calculations. Furthermore, it converged faster than the other frequency domain methods.

Shang et al. [13] developed a new theory for the application of local stress-strain field intensity to the fatigue damage at a notch. The effects of the local stress-strain gradient on fatigue damage were taken into account at notches. The parameters needed for local stress-strain intensity approach, as a fatigue analysis tool, were calculated from an incremental elastic-plastic finite element analysis under random cyclic loading. The method was especially used for detecting the

fatigue crack initiation life. It was verified with tests on a U-shaped notched specimen.

Kuntay et al. [14] studied the performance of accelerated life testing approach on an engine component of a vehicle. Finite element analysis of the structure was performed in order to determine the strain gage locations. Road load data was collected while traveling on Turkish roads and Lommel Proving Ground (LPG). The accelerated test profile was obtained by fatigue editing the collected data to decrease the test time. 1 million km road traveling accelerated life tests were performed in time domain to evaluate the design requirements of the structure. According to the feed back obtained from the accelerated life tests, structural modifications were applied on the critical parts in order to satisfy the fatigue requirements.

Hieber [15] investigated the advantages and disadvantages of Highly Accelerated Life Test (HALT) procedure. The main disadvantage is stated as the probability to cause failures which would not occur in the actual use of the product in the field. In order to have realistic life testing profiles, MIL-STD-810E encourages creating the profiles according to test measurements. It might be appropriate to increase the stress levels in steps not to cause a failure. In the study, a number of sample accelerated life testing calculations were given to show the increase in vibration levels due to decrease in test time. Furthermore, it is clearly shown that detailed information about the material should be available to determine the fatigue characteristics by accelerated life testing approach.

Consequently, critical conditions and important outcomes found in the literature are noted to be considered in this study. For example, mean and residual stresses from riveting may have a great role in fatigue lives of structures. In addition, multiaxiality is a condition which should be checked for loading. Furthermore, several equivalent stress methods are inspected and absolute maximum principal stress approach is decided to be the most appropriate one among them. Uses of cycle counting methods are seen and their results are discussed.

CHAPTER 3

FATIGUE THEORY

There are three basic categories in fatigue analysis. These are Stress Life, Strain Life and Crack Propagation methods. First one, the Stress life approach, is used where the stress levels are significantly below the yield stress. In this case, high number of cycles is required for failure. As a second method, Strain life approach is used where the material response to cyclic loading is strain rather than load controlled and results in plastic deformation. Finally, Crack propagation method is used when the size and shape of a pre-existing crack is known and the presence of the crack is critical for the structure. The propagation of the crack can be monitored by using this final method.

Stress life approach is adopted for the fatigue analysis considered in this study. The prominent features of the problem to be analyzed are; the presence of mean stresses, presence of different stress levels at different number of repetitions (which calls for a cycle counting method) and multiaxiality of loading. Because of the random vibration nature of the input loading which is spread over a wide frequency range, vibration fatigue method is also a viable tool to analyze the problem at hand.

Effect of mean stress on fatigue life of structures and Rainflow cycle counting method are given in APPENDIX A. In this chapter, Multiaxial Fatigue concept will be discussed in details since state of stress has a great influence on the fatigue life of structures. In addition, vibration fatigue method will be covered briefly.

3.1. Multiaxial Fatigue

Uniaxial cyclic loading is the focus of interest in the discussion of fatigue evaluations by stress life, strain life and crack propagation methods. However, many real design situations, including rotating shafts, connecting links, automotive and aircraft components and many others involve a multiaxial state of cyclic stress.

Therefore, many real design situations have more than one of the six stresses non-zero. In the simplest one of these cases, the stresses vary in simple proportion. Thus, directions of principal planes at any point remain constant with time. In the most general case they do not vary in a proportional way and at any point the directions of the principal stresses will vary during the cycle, as a function of time. In this case many different planes are candidates for the start of failure.

Loadings (stress responses) can therefore be classified as:

- Uniaxial,
- Multiaxial proportional,
- Multiaxial non-proportional.

There are different fatigue evaluation approaches for each of the above situations. This makes it important to determine which type of loading is the case. Uniaxial loading case is the easiest to determine. A typical stress vector for uniaxial loading, one principal stress-one direction, is given in Figure 3.1.

In order to distinguish the other two situations, proportional and non-proportional multiaxial loadings, new variables should be introduced and some checks should be performed. While studying multiaxial fatigue, it is important to make a distinction between multiaxial stresses and multiaxial loading. It is quite common to have more than one load application point (multiaxial loading), but at the same time have a uniaxial stress state because of the influence of geometry effects on the component.

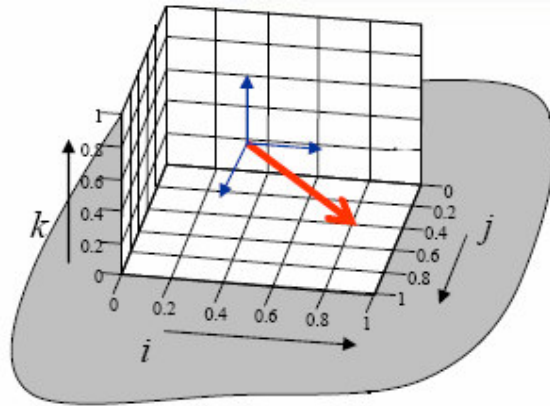


Figure 3.1: Stress vector of structures under uniaxial loading [16].

Two parameters used for determining the multiaxiality condition are defined as follows:

$$\text{Biaxiality Ratio} \quad a = \frac{\sigma_2}{\sigma_1} \quad (3.1)$$

Principal Stress Angle ϕ : Angle between σ_1 and x-axis

where;

σ_1, σ_2 : Principal stresses.

Proportional multiaxial case is defined as the condition in which biaxiality ratio and principal stress angle remains constant. On the other hand, biaxiality ratio and principal stress angle varies in non-proportional multiaxial loading.

Figure 3.2 to Figure 3.5 show principal stress versus biaxiality ratio and principal stress angle graphs for proportional and non-proportional multiaxial cases [17].

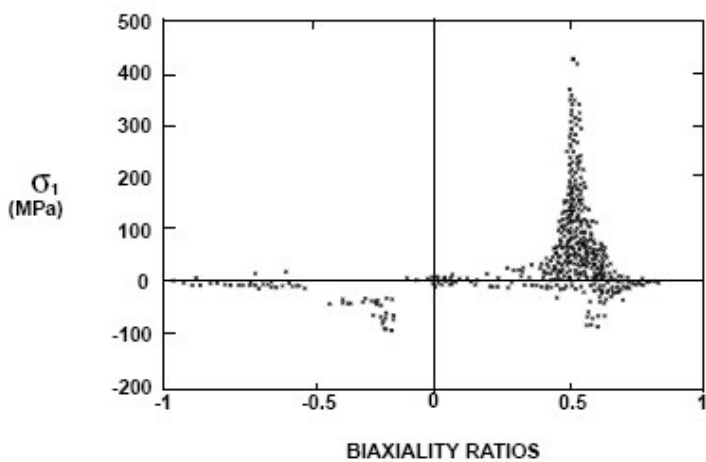


Figure 3.2: Principal stress vs. biaxiality ratio for proportional multiaxial loadings.

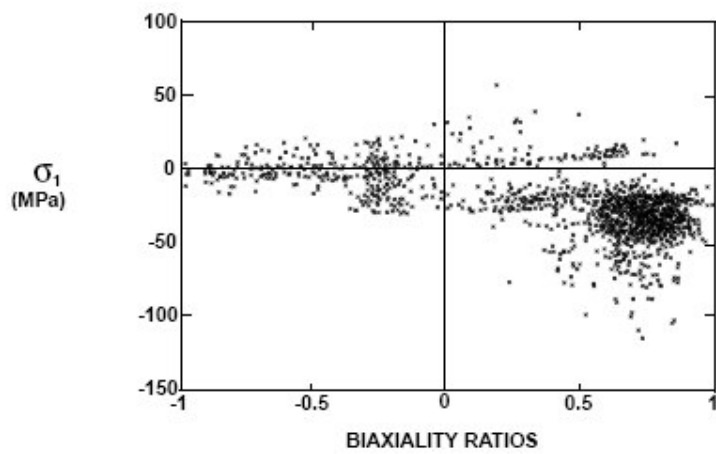


Figure 3.3: Principal stress vs. biaxiality ratio for non-proportional multiaxial loadings.

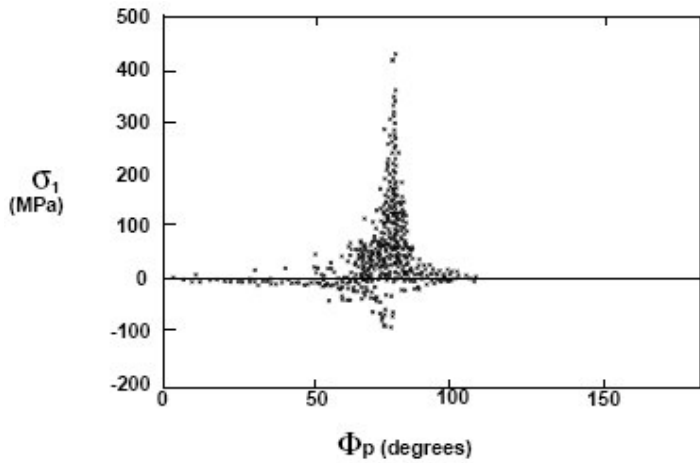


Figure 3.4: Principal stress vs. principal stress angle for proportional multiaxial loadings.

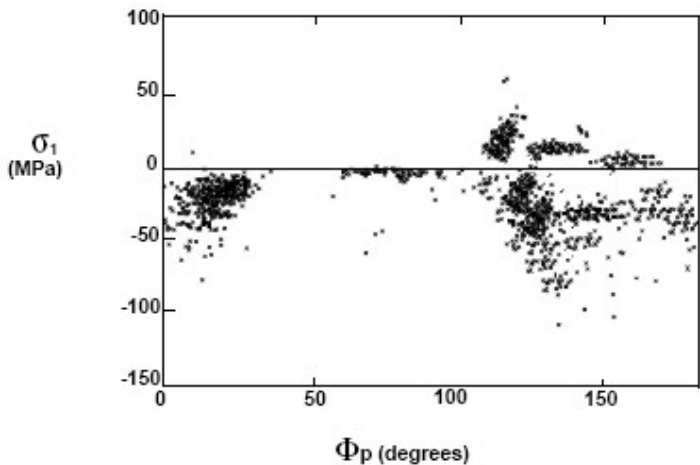


Figure 3.5: Principal stress vs. principal stress angle for non-proportional multiaxial loadings.

Using the states for the biaxiality ratio and principal stress angle, a determination can be made about the appropriate fatigue approach to use as follows:

Uniaxial	$\varphi = \text{constant}$	$a=0$	uniaxial theories
Proportional Multiaxial	$\varphi = \text{constant}$	$-1 < a < 1 = \text{constant}$	equivalent stress-strain
Non-proportional Multiaxial	$\varphi = \text{may vary}$	$a = \text{may vary}$	critical plane etc.

It is appropriate to discuss the methods used in proportional and non-proportional multiaxial cases at this point.

Equivalent stress-strain approaches are based on extensions to static yield theories. They assume that lifetimes for fatigue under multiaxial loading can be predicted by substituting combined stress or strain parameters in the uniaxial stress-life or strain-life equations (for example by calculating an equivalent uniaxial stress or strain for a given multiaxial loading). The main stress and strain parameters used are the maximum principal, the maximum shear (related to the Tresca criterion), and the von Mises or octahedral. The advantage of this kind of approach is that it enables the large amount of uniaxial fatigue test data available in the literature or in data banks to be applied to multiaxial situations [17].

Von Mises method has gained widest acceptance, but all these methods have drawbacks. In the Tresca criterion, the median principal stress does not affect the equivalent stress or strain, and neither of the von Mises or Tresca criteria varies with the application of a hydrostatic stress, contrary to experimental evidence.

Von Mises prediction of yield in terms of the principal stresses is

$$\sigma_0 = 0.7071 \left[(\sigma_1 - \sigma_2)^2 + (\sigma_2 - \sigma_3)^2 + (\sigma_3 - \sigma_1)^2 \right]^{0.5} \quad (3.2)$$

And yielding will occur when σ_0 exceeds the monotonic yield stress. In terms of the (x, y, z) component stress, it can be written as:

$$\sigma_0 = 0.7071 \left[(\sigma_x - \sigma_y)^2 + (\sigma_y - \sigma_z)^2 + (\sigma_z - \sigma_x)^2 + 6(\tau_{xy}^2 + \tau_{yz}^2 + \tau_{zx}^2) \right]^{0.5} \quad (3.3)$$

In order to perform a fatigue analysis, the equivalent (uniaxial) strain parameter that is used is as follows,

$$\varepsilon_0 = \frac{\sigma_1}{|\sigma_1|(1+\nu)\sqrt{2}} \cdot [(\varepsilon_1 - \varepsilon_2)^2 + (\varepsilon_2 - \varepsilon_3)^2 + (\varepsilon_3 - \varepsilon_1)^2]^{0.5} \quad (3.4)$$

As the name suggests, critical plane approaches recognize that fatigue damage (cracking) is essentially directional and so consider the accumulation of damage on particular planes. This is in contrast to the equivalent stress-strain approaches, which may be summing damage that is occurring on different planes. A range of methods for calculating damage on a particular plane are used. These methods include:

- Simply resolving the normal strain on the plane and applying what is essentially a uniaxial analysis.
- As above, but allowing for the multiaxial nature of the stresses through a consideration of the out-of-plane hardening.
- Variations on the Brown-Miller [17] approach, which consider the shear strain amplitude in the plane and the normal stress or strain.
- Typically, damage is calculated for all possible planes (at, say 10 degree intervals) and the worst or critical plane selected.

Most critical plane approaches use the Strain-Life damage method. However, there is one critical plane approach, the McDiarmid criterion, which uses a High Cycle Fatigue limit concept. Another fatigue limit approach, the Dang-Van Criterion, uses the maximum microscopic shear stress and the hydrostatic stress, as damage defining parameters [17]. Details of these approaches will not be covered since strain levels are low in this study and vibration fatigue method is more suitable.

3.2. Vibration Fatigue Approach

Generally, fatigue evaluation methods are time domain methods (Stress life, Strain life, Crack propagation). On the other hand vibration fatigue approach, which is a frequency domain approach, is used when the input loading or the

stress history obtained from the structure is random in nature and therefore best specified using statistical information about the process [18].

In order to obtain the response of the structure to random loading, frequency response functions are used. That is, when the system is linear then the response of the system will be the input multiplied by a linear frequency response function.

$$\text{Response}(f) = H(f) \times \text{Input}(f) \quad (3.5)$$

where,

$\text{Response}(f)$: Response FFT of the system

$H(f)$: Frequency response function of the system

$\text{Input}(f)$: Input FFT to the system

Frequency response function $H(f)$ of a system can be obtained by finite element modeling of the system and doing modal and harmonic analyses. Then the dynamic stress response under a given excitation can be obtained through Equation 3.5. Note that this method takes into account the dynamics of the system (natural frequencies and mode shapes) as opposed to calculating static stresses.

Once the stress response of the system is obtained the issue of damage accumulation can be addressed. Miner's linear damage accumulation model and S-N diagram equation is represented in random vibration theory as follows [17]:

$$E[D] = E[P] \frac{T}{C} \int_0^{\infty} S^b p(S) dS \quad (3.6)$$

where;

$E[D]$: Expected value of damage

$E[P]$: Expected number of peaks per second

T : Life in seconds

C : Material constant from S-N equation

b : Inverse slope of the Woehler curve

S : Stress amplitude

$p(S)$: Probability density function of Rainflow stress ranges

From this equation one can find the life of a component by setting the $E[D]$ equal to unity and obtain the life, T in seconds. For the integrations given above a cut-off value for the upper limit is necessary. This value is typically given in terms of Root Mean Square (RMS) values of stress. It is common to set the cut-off value to 3 RMS in amplitude or 6 RMS in range, but practice has shown that it should be at least set to 4.5 RMS in amplitude in order not to miss fatigue damage.

There are many empirical solutions for the Probability Density Function of Rainflow stress ranges, $p(S)$, like Tunna, Wirsching, Hancock, Chaudhury and Dover but the best correlation was obtained by Dirlik after extensive computer simulations to model random signals using the Monte Carlo method.

$$p(S_i) = \frac{\frac{D_1}{Q} e^{\frac{-Z_i}{Q}} + \frac{D_2 Z_i}{R^2} e^{\frac{-Z_i^2}{2R^2}} + D_3 Z_i e^{\frac{-Z_i^2}{2}}}{2\sqrt{m_0}} \quad (3.7)$$

where;

m_i : i^{th} moment of stress PSD

$$Z_i = \frac{S_i}{2\sqrt{m_0}}, \quad \gamma = \frac{E[0]}{E[P]}, \quad E[0] = \sqrt{\frac{m_2}{m_0}}, \quad E[P] = \sqrt{\frac{m_4}{m_2}}, \quad x_m = \frac{m_1}{m_0} \sqrt{\frac{m_2}{m_4}}$$

$$D_1 = \frac{2(x_m - \gamma^2)}{1 + \gamma^2}$$

$$D_2 = \frac{1 - \gamma - D_1 + D_1^2}{1 - R}$$

$$D_3 = 1 - D_1 - D_2$$

$$Q = \frac{1.25(\gamma - D_3 - D_2 R)}{D_1}$$

$$R = \frac{\gamma - x_m - D_1^2}{1 - \gamma - D_1 + D_1^2}$$

Calculation of spectral moment of stress PSD, mentioned above, is shown in Figure 3.6.

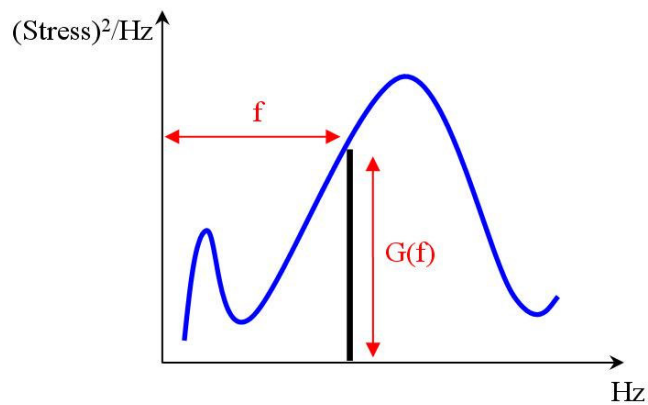


Figure 3.6: Spectral moment calculation of a stress PSD.

CHAPTER 4

ACCELERATED LIFE TESTING

Accelerated life testing of products and materials is used to get information quickly on their life distributions. Such testing involves subjecting the test units to conditions that are more severe than normal. This approach results in shorter lives than it would be observed under regular conditions.

Accelerated test conditions are typically produced by testing units at high levels of vibration, temperature, voltage, pressure, etc. It may also be a combination of the listed physical quantities.

The data obtained at more severe or accelerated conditions are extrapolated by means of an appropriate model to the normal conditions to obtain an estimate of the life distribution under normal conditions. Such testing provides a savings in time and cost compared with testing at normal conditions. In fact, operational life under normal conditions is so long that testing at those levels is not possible for many structures and materials. Vibration tests are performed by means of uniaxial or multiaxial shakers. Multiaxial vibration test equipment which consists of 8 shakers is shown in Figure 4.1.



Figure 4.1: An example of multiaxial vibration test equipment.

Although accelerated life testing gives useful information about the endurance of the systems, there are some drawbacks of this approach. Frequency domain accelerated life tests are only suggested for qualifying electronic equipments or their brackets and mechanical components such as cowling. Testing of large and heavy structures is not appropriate due to unstable or uncontrollable response of the structures and difficulties to fix them on the vibration systems.

There are two methods for determining the accelerated life testing vibration profiles,

- Frequency domain method
- Time domain method

In the following subchapters, these two methods will be briefly discussed. Frequency domain method will be covered in more details since it is the method used in this study.

4.1. Frequency domain method

Frequency domain method for synthesizing accelerated vibration profile requires PSD of the acceleration data as input. Real time data PSD is basically used as an exaggeration basis for building new PSD graphs with higher levels. Certainly, there are some criteria for the synthesis process.

There are two parameters used in synthesizing vibration profiles to separate the two failure mechanisms listed below.

Equipment subjected to vibration and shock may be damaged by two main mechanisms [19],

- When a stress generated by the loading exceeds a threshold,
- Fatigue accumulation damage due to fluctuating loading on the equipment.

Maximum Response Spectrum (MRS) is the first of the parameters mentioned above. When dynamic stress of any type is applied to a mechanical system with one degree of freedom for a given duration, the reference system responds by a relative displacement of the mass with respect to the base. The maximum amplitude (z) of the relative displacement depends on the natural frequency (f_0) of the reference. In addition, it is proportional to the maximum stress induced in the spring.

The curves showing the variations in $4\pi^2 f_0^2 z$ versus frequency f_0 for a specified damping ξ is called “Maximum Response Spectrum”. In the case where shock is the loading, MRS is the primary shock spectrum.

On the other hand, “Fatigue Damage Spectrum” is the curve representing the variation in damage D versus f_0 for given values of ξ and b , where b is the inverse slope of the Woehler curve.

Using the definitions of Woehler curve, stress-strain definitions with Miner’s rule gives the following equation:

$$D = \frac{K^b}{C} \sum_i n_i z_i^b \quad (4.1)$$

where,

K: Constant value relating stress with displacement,

n: Number of cycles in the histogram,

z : amplitude of the displacement.

Having defined MRS and FDS parameters, the use of them in an operational process (such as max. power climbing and autorotative glide missions in a helicopter flight scenario) is as follows:

- For events occurring in parallel (max. power climbing OR autorotative glide)
 - Envelope of the MRSs
 - Envelope of the FDSs
- For events occurring in series (max. power climbing AND autorotative glide)
 - Envelope of the MRSs
 - Sum of the FDSs

The main progress cycle of frequency domain method is shown in Figure 4.2.

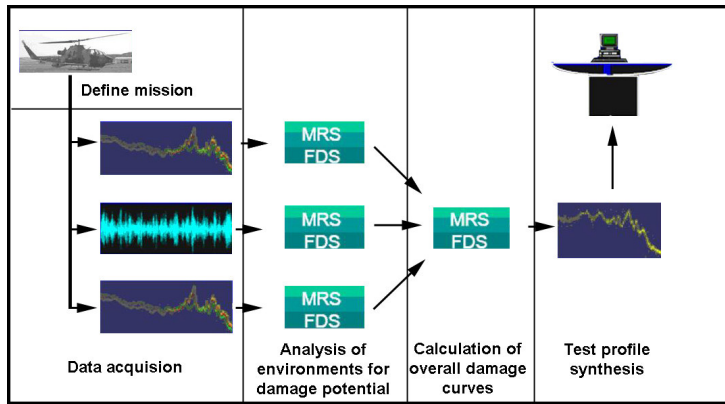


Figure 4.2: Frequency domain synthesis [2].

Most of the time, it is clear what the most probable cause of failure is going to be according to the application: fatigue or exceeding stress levels. This will determine which damage curve should be used as a criterion for the synthesis. However, it is always necessary to evaluate the other damage curve as well.

If fatigue failure type of vibration profile is synthesized, test time will be reduced most probably. Therefore, it may induce unrealistically high peak levels in the system, causing the failure mechanism to shift from fatigue to overstress. This can be evaluated by calculating the MRS curve from the obtained PSD or swept sine profile and comparing this to the MRS of the life profile.

The advantages of frequency domain method over time domain method are:

- Accelerated test duration can be reduced much more
- It requires less disk space for the input file
- Broadband vibration capability

4.1.1. Frequency domain approaches in International Military Standards

There are some international standards for determination of the appropriate vibration profile to be used for tracked vehicles, helicopters etc. General rules and approximations on frequency domain vibration level exaggeration are also included. However, they only give an idea about the vibration levels.

One of the widely used military standards, MIL-STD-810F [20], states the importance of experimentally obtained vibration level of helicopters in Method 514.5 Category 14 page 514.5A-9 as, “Vibration levels and spectrum shapes vary widely between helicopter types and throughout each helicopter, depending on strength and location of sources and the geometry and stiffness of the structure. Thus, the need for measured data is acute.”

According to ITOP,[21], “The ratio of ultimate stress (U) to the elastic limit (Y) and ultimate stress (U) to the endurance limit (EN) were calculated for each of the metals and averaged, producing values of $U/Y=1.37$ and $U/EN=2.78$. These ratios were then averaged, producing a value of 2.08. The value of 2 is therefore suggested as the maximum limit for exaggeration factor”.

Exaggeration factor is defined as the amplitude ratio of the accelerated vibration profile to the original vibration profile (W_2/W_1).

MIL-STD-810E [22] states that the standard equations are simplified versions and do not represent the nonlinear behavior of the structures. Therefore, the validity of these equations is questionable. Nonlinear characteristics of structures

are critical when broad band random loading is the case, since loading would excite the natural modes.

It is stated that PSD level at each frequency has a simple relationship with the accelerated life test duration, which is derived as follows:

$$N \cdot \sigma^b = \text{constant} \quad (4.2)$$

$$N = f_n \cdot t \quad (4.3)$$

where,

f_n : Natural frequency of the SDOF system

t: Applied duration

It is stated that vibration acceleration input (W) and stress response (σ) level which is nonlinear is related by a constant “n” [15].

$$\sigma \propto W^{1/n} \quad (4.4)$$

By combining equations 4.3 and 4.4 with equation 4.2,

$$f_n \cdot t \cdot W^{b/n} = \text{constant} \quad (4.5)$$

Equation 4.5 can be used for two separate test scenarios.

$$f_n \cdot t_1 \cdot W_1^{b/n} = f_n \cdot t_2 \cdot W_2^{b/n} \quad (4.6)$$

By canceling the common elements and dividing side by side, equation 4.7 is obtained.

$$\left(\frac{W_1}{W_2} \right)^{\frac{b}{n}} = \frac{t_2}{t_1} \quad [21] \quad (4.7)$$

in which,

W_1 : Real time PSD amplitude (g^2/Hz)

W_2 : Laboratory test PSD amplitude (g^2/Hz)

t_1 : Real time (hour)

t_2 : Test time (hour)

b: Inverse slope of the Woehler curve

n: Stress damping constant

The standards recommend certain methods to improve the efficiency of the study. However, it is known that the best approach is to test the actual structure and perform the exaggeration operation accordingly.

4.2. Time domain method

Time domain method directly uses the collected time data for the synthesis process. The most commonly used physical quantity used is acceleration. This method is mainly used in automotive industry, since it is assumed that loading is independent of frequency and quasi-static.

The methodology used in time domain is basically elimination procedure. Tailoring is done on the time data which has low amplitude. The amount of data which would create low fatigue damage is eliminated so that the test duration is reduced. While doing that, the remaining data is increased so that the total damage is kept constant with the original data [16].

Figure 4.3 shows a sample original real time data and the portions to be eliminated (green). The remaining data after tailoring is seen in Figure 4.4.

The main advantage of time domain method over frequency domain is the ability to keep the phase information of loadings. This means that the sequence of the loading is taken into account in time domain method. On the other hand, it is simulated as a random loading in frequency domain method.

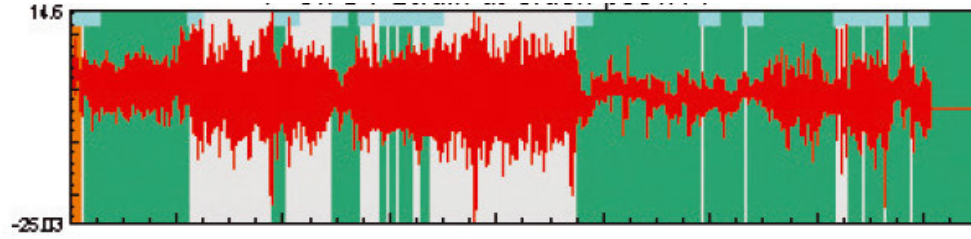


Figure 4.3: A sample original time data before tailoring [16].

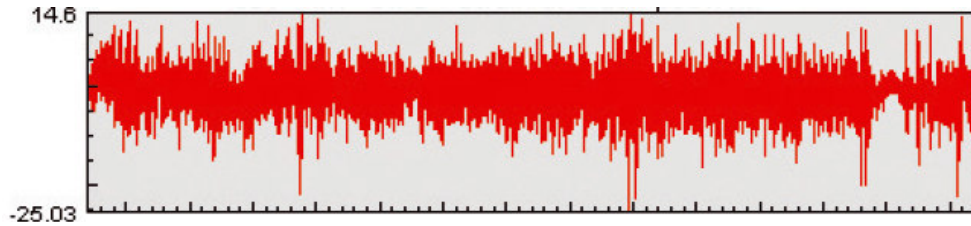


Figure 4.4: Data after tailoring [16].

Time domain profiling procedure can be summarized at this point. After collecting the data at the critical locations, total damage is calculated. Profile synthesis is performed by tailoring the data. Numerical methods are used for transferring the new profile to the structure. Response of the structure is obtained by the numerical analysis. Rainflow counting is used for determining the modified damage. In order to keep the total damage constant, data level is adjusted. The final profile is applied to the structure experimentally by means of shakers etc.

CHAPTER 5

OPERATIONAL FLIGHT TESTS AND MISSION SYNTHESIS

5.1. Operational Flight Tests and Data Acquisition

Stress histories of specific locations are required to perform fatigue analysis of the structures. Operational tests can be used directly or indirectly for this purpose. If the component is mounted on the platform where it functions, operational tests can be used directly to obtain the stress history. On the other hand, if the component is at the design stage, operational tests can be used indirectly by applying the environmental conditions, measured during the tests, on the prototype by means of an electro-dynamic shaker.

Another way of using an electro-dynamic shaker as an indirect tool for tests is the application of military standards (MIL-STD-810F, GAM EG13). The standards have vibration profiles corresponding to several platforms (land, naval, aerospace). However, the profiles in the standards are very coarse and they are built to give an approximate level of vibration. Therefore, they should only be used when testing of a specific platform is not possible. The standards strongly recommend determining the vibration test profiles by testing the actual platform under its working conditions wherever possible.

Indirect application of operational tests is used in this study, since the Missile Warning Sensor (MWS) is at the design stage and the actual unit is not mounted on the helicopter yet. In other words, operational flight tests are performed for acceleration data acquisition at the mounting location.

In Figure 5.1, AH-1P helicopter is shown during operational flight tests.



Figure 5.1: AH-1P helicopter during operational tests.

A flight profile which was prepared by test pilots and engineers is used for the operational tests. The profile includes rough maneuvers as well as steady flight which will be experienced by the helicopter during its operational life. The applied flight profile is given in APPENDIX B.

Tri-axial Integrated Circuit Piezoelectric (ICP) accelerometers of 50g amplitude are used for measuring the vibration level of the desired locations on the helicopter. Operation principle of ICP accelerometers is explained in APPENDIX C. Typical triaxial ICP accelerometers are shown in Figure 5.2.

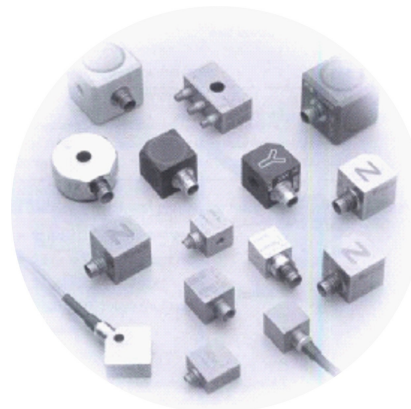


Figure 5.2: Triaxial ICP accelerometers [23].

Locations of the accelerometers to be placed on the helicopter are determined according to possible mounting points of several units. Missile Warning Sensor (MWS) is one of the units planned to be integrated on the helicopter. In Figure 5.3, location of the accelerometer on the helicopter's MWS mounting point is shown.

The possible points of mounting are determined by considering the maximum effectiveness of the units. The effectiveness of MWS is very important to identify the missiles approaching all around the helicopter. The effective area scanned by the MWS is shown in Figure 5.4.

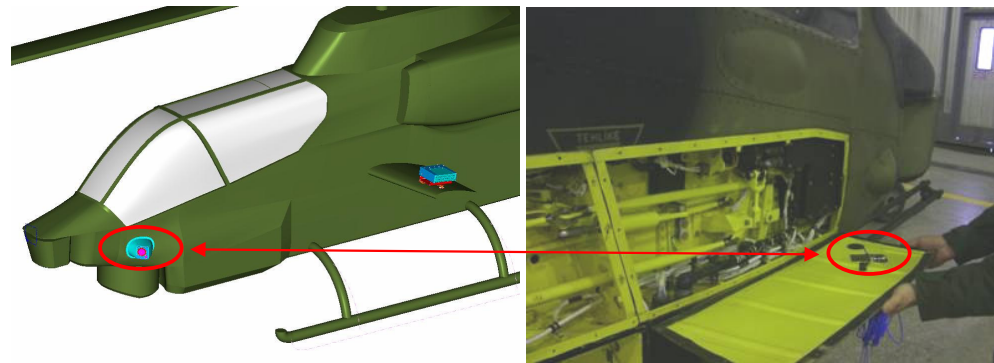


Figure 5.3: Accelerometer location at the MWS mounting region of the helicopter.

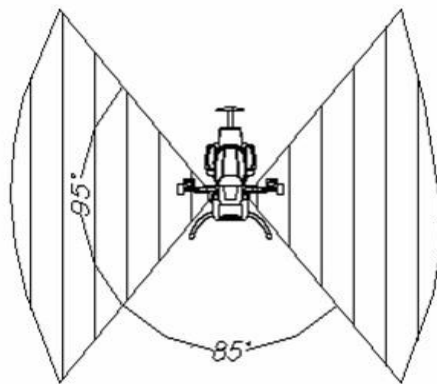


Figure 5.4: Effective area scanned by the MWS.

ESA Traveller Plus [24] data acquisition system with 32 channels is used for the operational flight tests. The location of the system in the helicopter is given in Figure 5.5. A sampling rate of 5000 Hz is set (analysis frequency 2500 Hz) for the accelerometers. The flight profile given in APPENDIX-B is flown continuously and data is stored accordingly.



Figure 5.5: Location of the data acquisition system during the flight tests.

Figure 5.6 to Figure 5.8 show the acceleration versus time signals collected at the MWS mounting location in three axes.

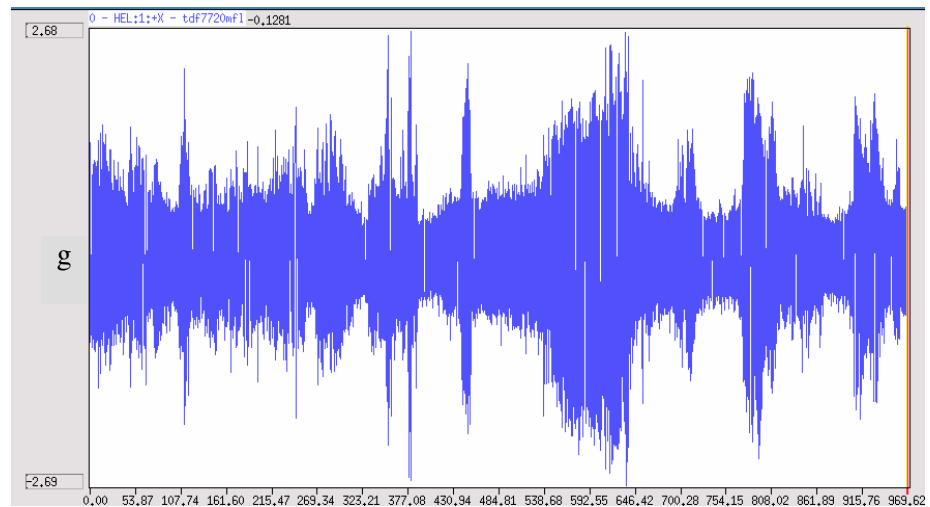


Figure 5.6: Acceleration-time data collected at the MWS location, longitudinal (X) axis.

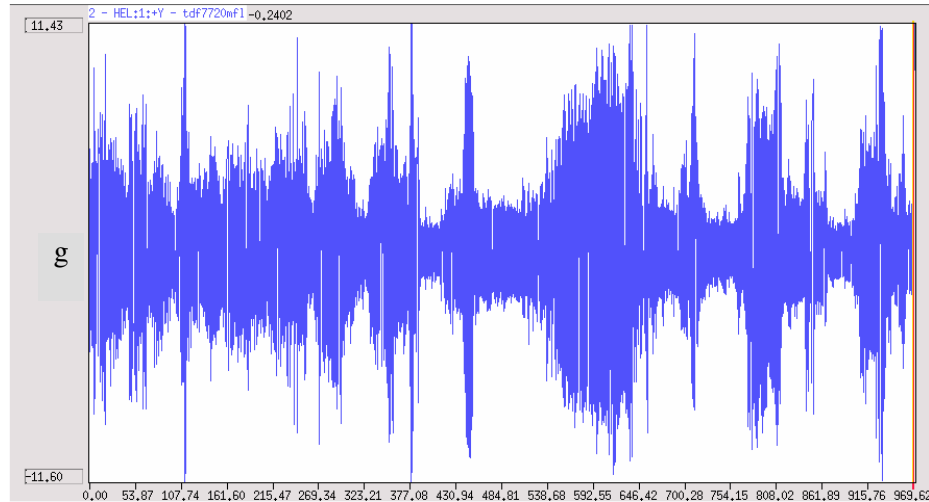


Figure 5.7: Acceleration-time data collected at the MWS location, vertical (Z) axis.

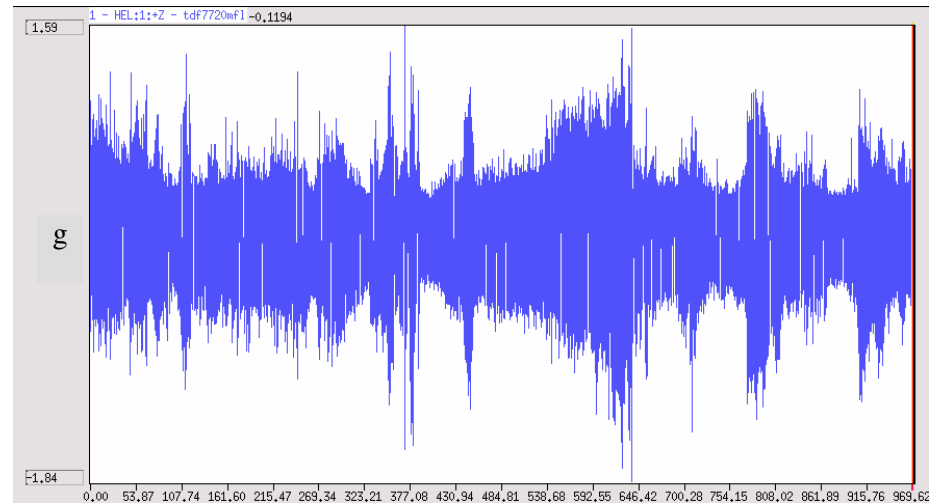


Figure 5.8: Acceleration-time data collected at the MWS location, transverse (Y) axis.

Note that the maximum acceleration level is obtained in vertical (Z) direction.

Power Spectral Density (PSD) graphs of the time signals are given below.

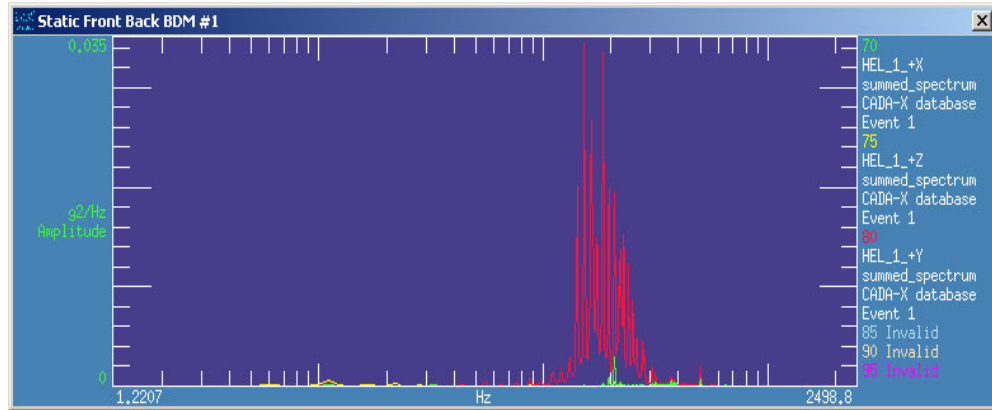


Figure 5.9: PSD graphs in all directions (green: longitudinal, yellow: vertical, red: transverse).

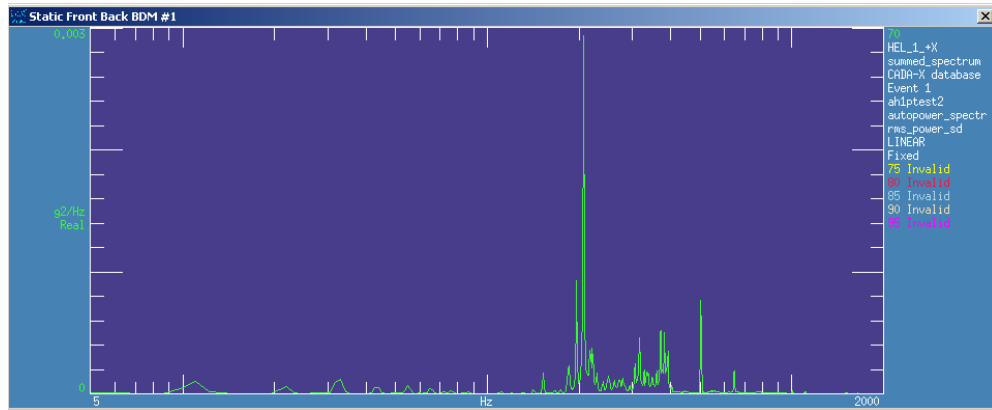


Figure 5.10: PSD graph in longitudinal (X) axis.

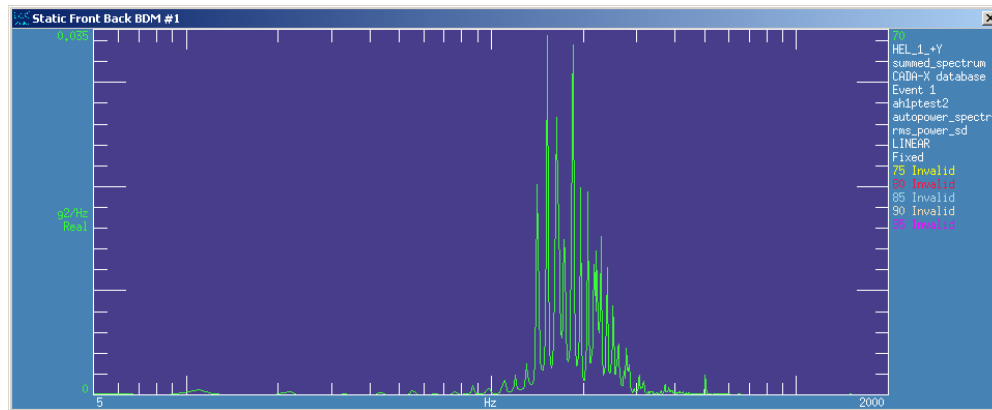


Figure 5.11: PSD graph in vertical (Z) axis.

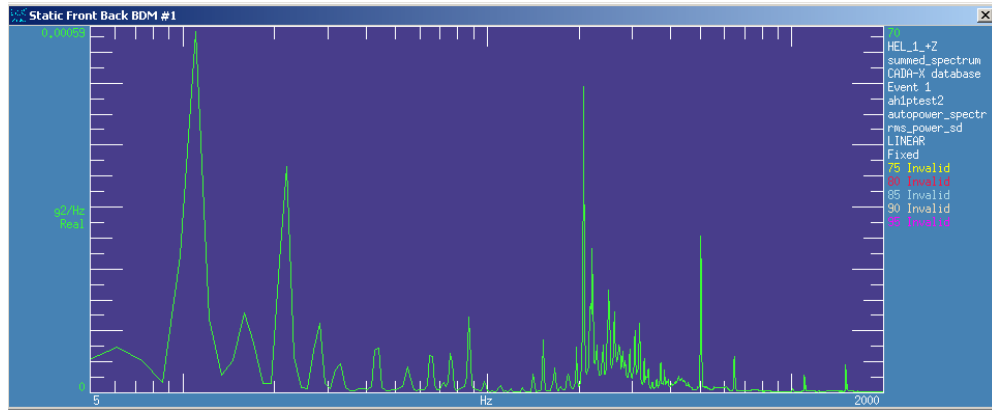


Figure 5.12: PSD graph in transverse (Y) axis.

Note that the vertical axes of the plots have different scales for X,Z and Y axis loadings. The magnitude of the PSD of acceleration in transverse (Y) direction is actually much smaller. It is seen that frequency distribution in transverse axis is more spread out than the other two axes. Higher frequencies are dominant in longitudinal and vertical axes.

5.2. Mission Synthesis of Operational Data

In order to obtain functional and endurance vibration profiles for loading the structure that is measured during operation, mission synthesis process should be performed. Vibration profiles can be synthesized with the reference PSD given in Figure 5.10 to Figure 5.12. The reference PSD is used as an exaggeration basis for creating new accelerated vibration profiles.

Since MWS component is expected to have 12000 hours of functional life, the data collected during operational flight tests is considered as a reference data which corresponds to 12000 hours. Therefore, PSD of the operational data is used as a reference PSD.

In the study, total of four vibration profiles are synthesized per axis. These profiles correspond to accelerated profiles of 1 hour, 4 hours, 100 hours and 3000

hours. The vibration profile corresponding to 4 hours will be used for accelerated life test of the MWS for fatigue testing. In addition, all of five vibration profiles (1 hour, 4 hours, 100 hours, 3000 hours and 12000 hours) will be used for experimental stress analysis of the structure.

LMS Mission Synthesis software [2] is used for mission synthesis processes. There are some parameters used to perform mission synthesis. First of all, MRS/FDS, which are the shock and vibration content of the raw signal respectively, should be calculated using the reference PSD. While doing this, the damping of the single degree of freedom system (Q), the inverse slope of the Woehler curve (b), situation parameter (time duration) and frequency band are used as inputs (Figure 5.13).

"Q" value is taken as 10 for lowly damped structures and "b" is chosen as 6.4 for aluminum 2024-T3. These values are material constants and they are selected according to the suggested values by LMS and references for experimentally determined aerospace applications [25]. Other material parameters, A and K are not relevant to this analysis and can be left as 1 in the software. "Total time" is set to 12000 hours as a customer specification. Frequency range is set at 5-2000 Hz, with increments of 1 Hz.

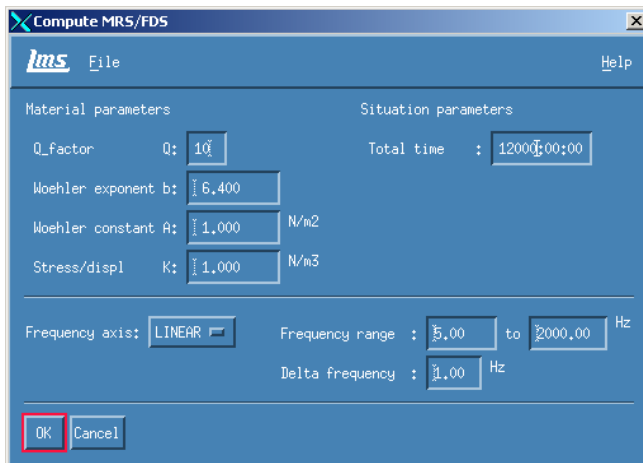


Figure 5.13: MRS/FDS calculation window.

After processing MRS/FDS, it is recalled that FDS is the cumulative nature of the fatigue mechanism. Hence, new profile is synthesized by using the FDS content. Figure 5.14 shows the window for the profile synthesis. In this window, excitation type and the test duration is used, and other parameters are set from the previous window. Therefore, PSD is used as the excitation type in this study. Test duration determines how long the synthesized profile will be applied to the structure (it is set to 4, as an example) during accelerated life tests.

Due to uncertainty of the data collected, which are number of tests, confidence level and material variation, a test factor is applied on the new synthesis profile. The uncertainty parameters used in this section is shown in Figure 5.15. These values are selected according to LMS suggestions and experimentally acceptable aerospace parameters for such applications.

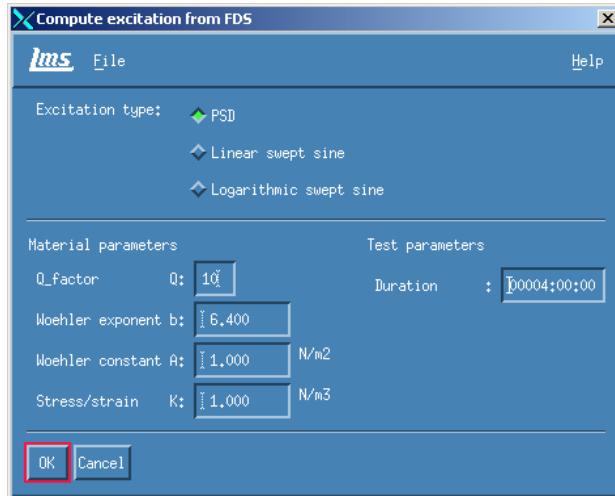


Figure 5.14: Profile synthesis window.

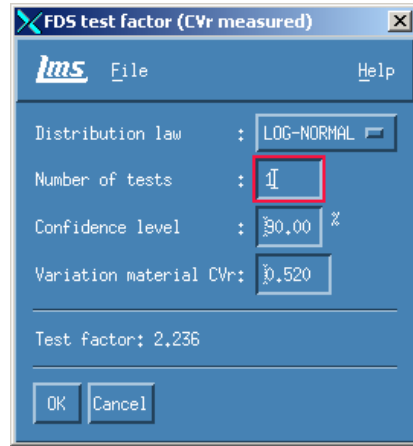


Figure 5.15: Test factor evaluation window.

The comparison of the profiles synthesized for 1 hour, 4 hours, 100 hours, 3000 hours and 12000 hours of test duration is shown in Figure 5.16. It is seen that, frequency contents of the profiles are the same, whereas, amplitudes are increasing according to the signal content by decreasing test duration.

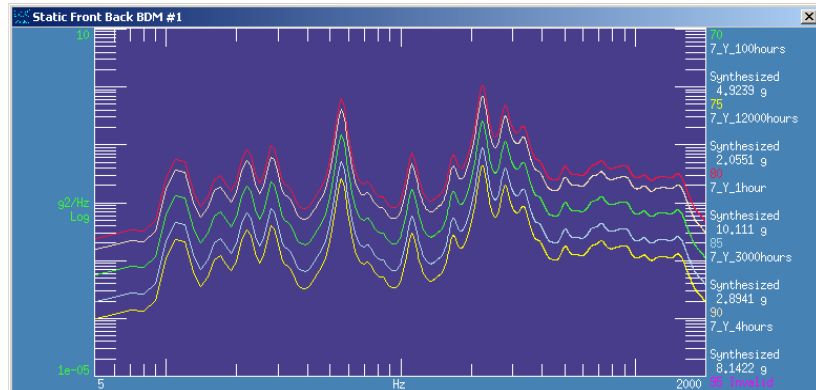


Figure 5.16: Comparison of the synthesized PSD profiles (Y axis).

These profiles are run in the vibration test equipment for qualification of the structures. In order to drive the shaker by the profiles synthesized, they should be in a discrete form. This is done by snap clicking on critical points on the curve so

that the original curve can be represented by connecting these points by lines. Verification of the correctness of these points can be done by plotting the original curve and the edited curve on the same graph, as shown in Figure 5.17.

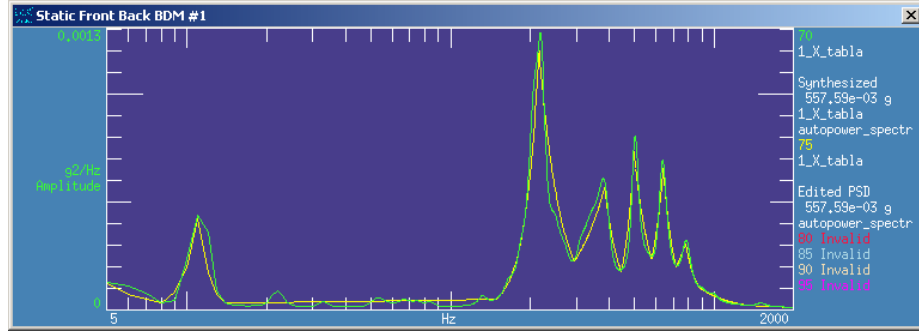


Figure 5.17: Comparison of original profile with the edited profile (X axis).
(green: original profile, yellow: edited profile)

After verification, coordinates of the points selected (frequency vs. amplitude) can be obtained to be used as an input to the shaker. A sample input table is shown in Figure 5.18.

random PSD				
Rms value : 557.59e-03 g				
Editor lines : Frequency Left slope Amplitude Right slope				
[Hz]	[dB]	[g2/Hz]	[dB]	
5.00	-----	120.2e-06	-----	
8.01	-----	33.62e-06	-----	
11.00	-----	420.1e-06	-----	
14.07	-----	32.56e-06	-----	
148.34	-----	49.43e-06	-----	
216.68	-----	1.207e-03	-----	
294.62	-----	225.8e-06	-----	
384.51	-----	570.5e-06	-----	
443.79	-----	179.2e-06	-----	
496.71	-----	734.3e-06	-----	
579.20	-----	237.8e-06	-----	
641.66	-----	657.2e-06	-----	
718.18	-----	198.1e-06	-----	
779.50	-----	308.5e-06	-----	
872.46	-----	107.8e-06	-----	
1355.21	-----	21.19e-06	-----	
2000.00	-----	12.08e-06	-----	

Figure 5.18: Typical input table for a PSD driven shaker.

The accelerated life testing profiles for 4 hours test duration for longitudinal, vertical and transverse axes are given in Figure 5.19 to Figure 5.21.

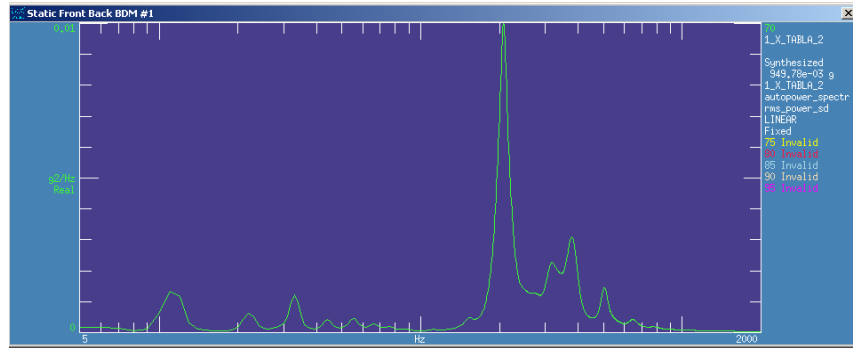


Figure 5.19: Accelerated life testing profile, longitudinal axis.

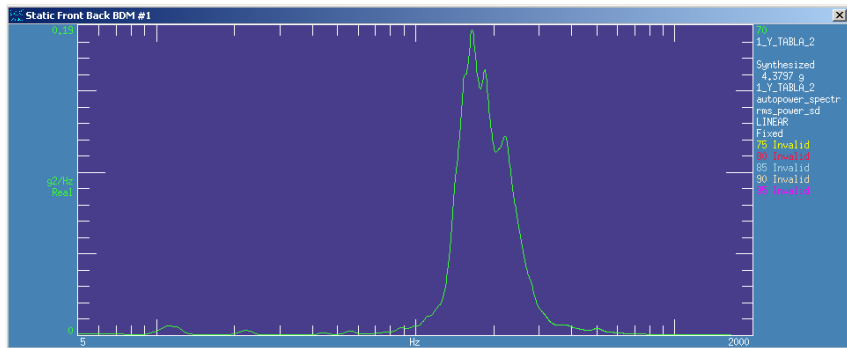


Figure 5.20: Accelerated life testing profile, vertical axis.

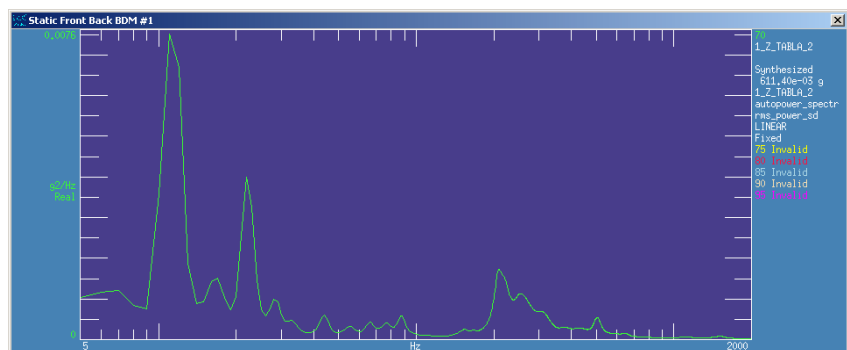


Figure 5.21: Accelerated life testing profile, transverse axis.

CHAPTER 6

NUMERICAL AND EXPERIMENTAL FATIGUE ANALYSIS OF MWS-COWLING ASSEMBLY

Fatigue analysis of structures can be performed by two basic methods. These are Numerical Fatigue Analysis and Experimental Fatigue Analysis. Numerical Analysis can be used as an assisting study for Experimental Analysis by means of pointing out the critical locations. On the other hand, Experimental Analysis can be used to correct the model used in Numerical Analysis.

6.1. Numerical Fatigue Analysis of MWS-Cowling Assembly

Dynamic response characteristics of the structure should be known in order to perform Numerical Fatigue Analysis. This need can be satisfied by performing Harmonic Analysis of the structure. Harmonic Analysis gives the frequency response functions of the structure in frequency domain as an output. Harmonic Analysis requires a finite element model and a modal analysis solution.

Numerical (finite element) model of the MWS-cowling assembly is created in ANSYS [26] environment with 11309 elements and 34764 nodes (Figure 6.1). SHELL91 element is used for building the cowling portion and MASS21 element is used for representing the MWS as a mass element. Cowling has a thickness of 1 mm and stiffeners have 1 mm thickness as well. The thicknesses are defined by shell element settings. Inertia and mass properties of the MWS is defined in mass element settings. MWS and its composite bracket have a total mass of 2.6 kg.

Mass element is connected to shell elements by rigid regions at the rivet connection holes of the physical prototype.

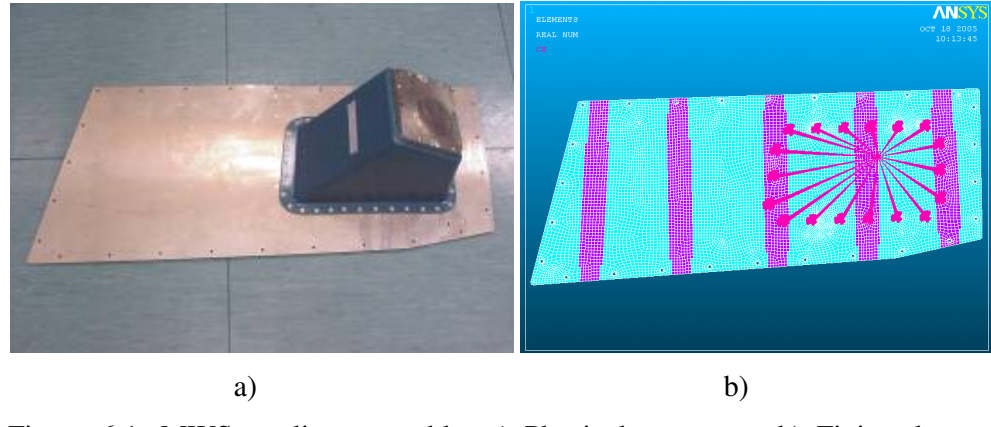


Figure 6.1: MWS-cowling assembly, a) Physical prototype, b) Finite element model.

Boundary conditions of the assembly applied on the finite element model are shown in Figure 6.2 and they are defined as follows:

- Bolt holes have fixed boundary condition in all directions,
 - Lower edge of the cowling has only rotation about itself free,
 - Rest of the cowling edges has translation constraints due to neighbor cowling portions (upper edge in upwards direction, left hand side edge in leftward direction, right hand side edge in rightward direction).

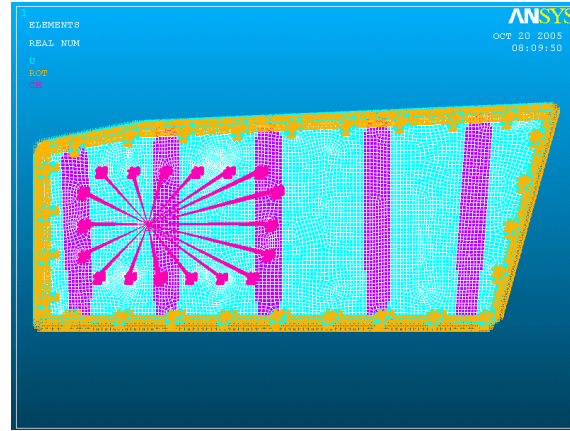


Figure 6.2: Boundary conditions on the assembly.

Modal analysis of the assembly is performed for first 10 modes, approximately up to 360 Hz (Figure 6.3). This mode information is used as an input to harmonic analysis. First mode shape of the assembly at 76 Hz is shown in Figure 6.4.

***** INDEX OF DATA SETS ON RESULTS FILE *****					
SET	TIME/FREQ	LOAD	STEP	SUBSTEP	CUMULATIVE
1	76.038		1	1	1
2	82.323		1	2	1
3	90.816		1	3	1
4	124.10		1	4	1
5	154.74		1	5	1
6	237.97		1	6	1
7	278.58		1	7	1
8	295.55		1	8	1
9	332.56		1	9	1
10	358.41		1	10	1

Figure 6.3: First 10 natural frequency of the assembly (ANSYS [26] output).



Figure 6.4: First mode shape of the MWS-cowling assembly (76 Hz).

Harmonic analysis of the structure is done in each axis up to 2000 Hz with a resolution of 4 Hz. A total of 17 frequencies are expanded. 10 of them are the first 10 natural frequencies of the assembly. The remaining 7 frequencies are determined by inspecting the peak values on the PSD graphs of the data collected in operational tests (12 Hz, 16 Hz, 20 Hz, 32 Hz, 160 Hz, 208 Hz and 216 Hz). The harmonic analysis results file, created in ANSYS [26] is read by MSC Fatigue [17] software for each frequency. MSC Fatigue [17] software will be used for the numerical fatigue analysis.

Harmonic analysis result at a frequency gives a frequency response function that will be used in numerical fatigue analysis. It is also a measure of how the structure behaves under a sinusoidal loading with 1g amplitude at a given frequency. Damping is taken as 1% as a typical value for aluminum applications.

In Figure 6.5, von Mises stress distribution on the cowling is given as a result of harmonic analysis at its first natural frequency (76 Hz) in transverse direction. Maximum von Mises stress is found as 51.6 MPa at one of the hole edges, as shown in Figure 6.6.

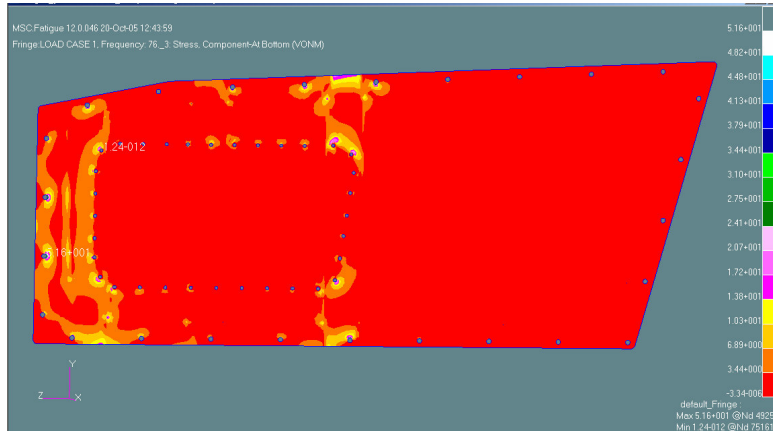


Figure 6.5: von Mises stress distribution of 76 Hz harmonic analysis solution.

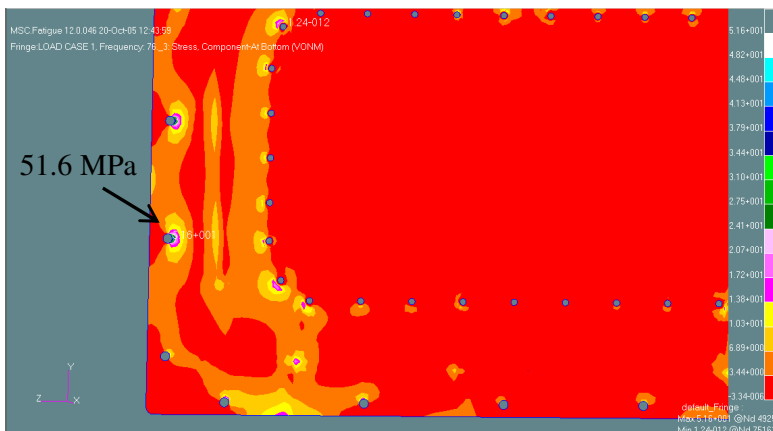


Figure 6.6: Location of the maximum stress region.

PSD and cross PSD of the time data collected in operational flight tests at the MWS mounting location is used as loading in three axes. These are defined in MSC Fatigue [17] loading menu in a matrix form as shown in Table 6.1.

Table 6.1: Frequency response functions and PSD Loading Table.

Frequency Response Cases	# of Frequency Response	PSD matrix (i,1)	PSD matrix (i,2)	PSD matrix (i,3)
1	17 (01:17)	X axis PSD	X-Y axis cross PSD	X-Z axis cross PSD
2	17 (18:34)	X-Y axis cross PSD	Y axis PSD	Y-Z axis cross PSD
3	17 (35:51)	X-Z axis cross PSD	Y-Z axis cross PSD	Z axis PSD

Material S-N data is used as it is defined in MSC Fatigue software for Aluminum 2024-HV-T3 (Figure 6.7).

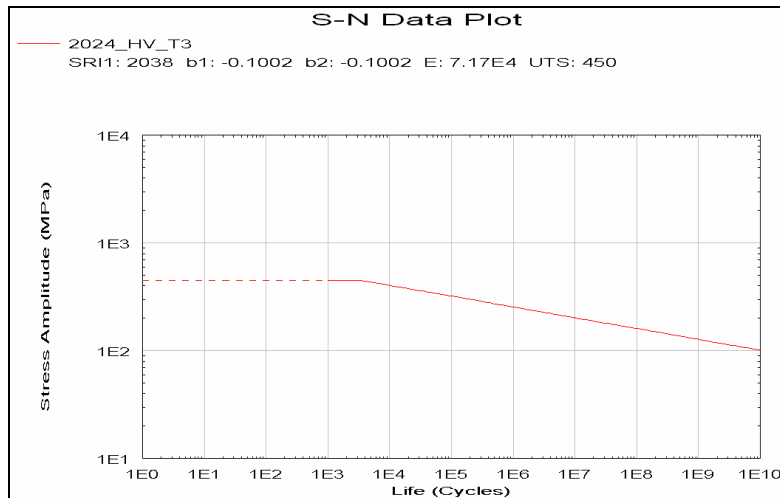


Figure 6.7: S-N curve of 2024-HV-T3 material [17].

Numerical fatigue analysis is performed by applying Dirlik's method as a vibration fatigue solution technique, explained in Chapter 3.2. Maximum absolute principal stresses are used for evaluating the fatigue damage. Three dimensional

PSD loading is applied as a multiple loading. This means that they are taken into consideration as simultaneous acting loadings, which is the real case.

Results of the numerical fatigue analysis are given in the following two figures. Locations with maximum and minimum life are shown in Figure 6.8, and a close view of the most critical region, with 2.32×10^{16} seconds (6.44×10^{12} hours) operational life, which can be considered as infinite life for aluminum structures, is shown in Figure 6.9.

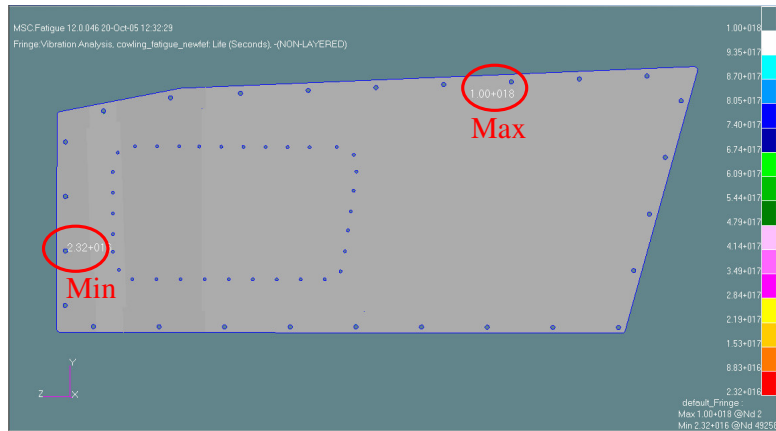


Figure 6.8: Locations with maximum and minimum fatigue life.

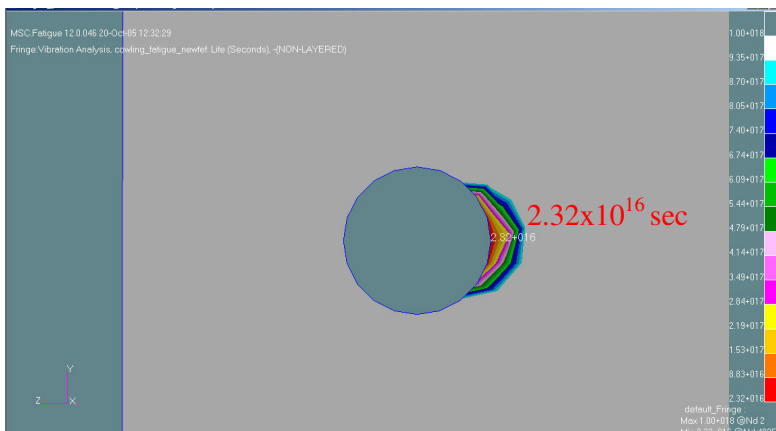


Figure 6.9: The most critical location-closer view (minimum fatigue life).

It should be noted that location with minimum fatigue life is the same as the location with maximum von Mises stress obtained in harmonic analysis.

6.2. Experimental Fatigue Analysis of MWS-Cowling Assembly

Experimental fatigue analysis is essential in a way that the finite element model needs to be verified. In addition, if the life of the structure is suspected to be less than the minimum requirements, stress analysis at the critical locations should be performed.

Three rectangular rosettes, CEA-13-250R-350 [27], are glued on the cowling portion of the assembly, since that portion is the interest of this study. Location of the first strain rosette is the most critical region determined by the numerical fatigue analysis. Second strain rosette is placed at the most deflecting point for the first mode of the assembly, as previously given in Figure 6.4. Finally, third strain rosette is glued on the further edge to the MWS. Exact locations of the strain rosettes are shown in APPENDIX-I. Furthermore, a total of four triaxial ICP accelerometers are placed next to the rosettes and at the tip of MWS. Sensor locations are given in Figure 6.10.

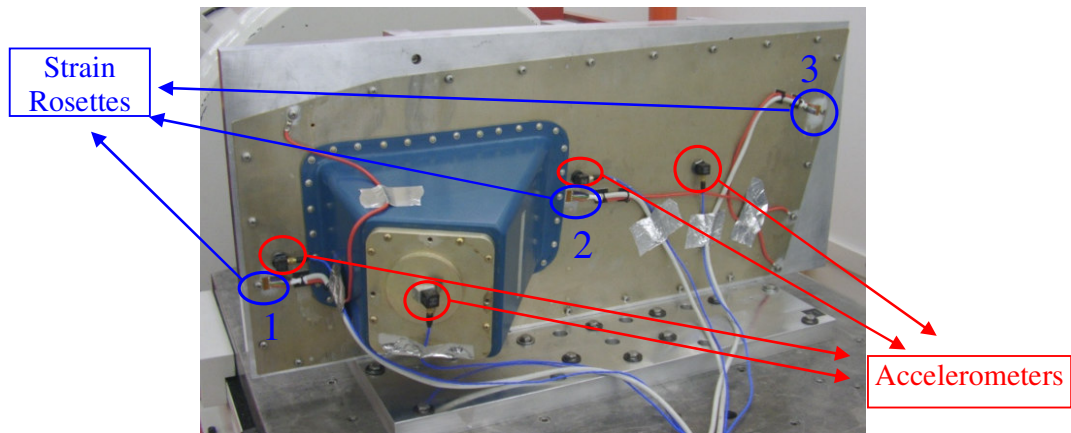


Figure 6.10: Sensor locations on the assembly.

The tightening torque of the M5 bolts that are used to mount the cowling to the helicopter body was not specified by the army. Therefore, a bolt analysis is performed to determine the optimum tightening torque to be used in the experimental analysis. Structure is modeled in HEXAGON-SR1 [28] software by specifying the effective area, bolt type, washer and the members (Figure 6.11).

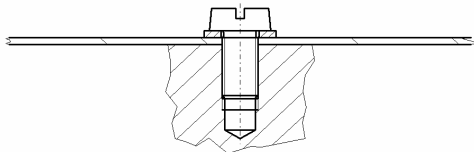


Figure 6.11: Bolt analysis model prepared in HEXAGON-SR1.

The outcome of the analysis was that the torque should be selected in the range of 2-4 N.m. Thus, 3 N.m is selected as the tightening torque for the M5 bolts with the fixture. Furthermore, this bolt analysis reveals that the assembly stresses are at safe levels. The full analysis sheet is given in APPENDIX D.

A special fixture is manufactured for fixing the assembly on the shaker (Figure 6.12). The design of the fixture is very important in a way that it should be as rigid as possible but light in weight. This is required for correctly (directly) transferring the vibration energy from shaker head to the structure.



Figure 6.12: Aluminum fixture for connecting shaker and the assembly.

Before starting the full endurance tests (4 hours accelerated tests applied for 4 hours) in three axes, 1 hour, 4 hours, 100 hours, 3000 hours and 12000 hours accelerated tests are performed in three axes for 10 minutes, by using the vibration profiles determined in Chapter 4.2. Data is recorded from the sensors during this 10 minutes period run. This data will be analyzed in the following chapter.

After collecting data from the healthy structure, endurance tests are started. Tests are performed by using vibration test equipment (shaker) [29] in ASELSAN Environmental Testing Laboratories (Figure 6.13). The system has a closed-loop control system and it is driven by PSDs.

Positions of the MWS-cowling assembly on the shaker, during the tests, in three axes are shown in Figure 6.14.

During and after the tests in each axis, detailed visual inspections are done on the assembly and no failure is observed. Hence, it is assured that the MWS-cowling assembly will serve at least 12000 operational hours without any failure. However, actual life and the most critical region of the unit are not determined, since there was no failure observed.



Figure 6.13: Vibration test laboratory in ASELSAN.

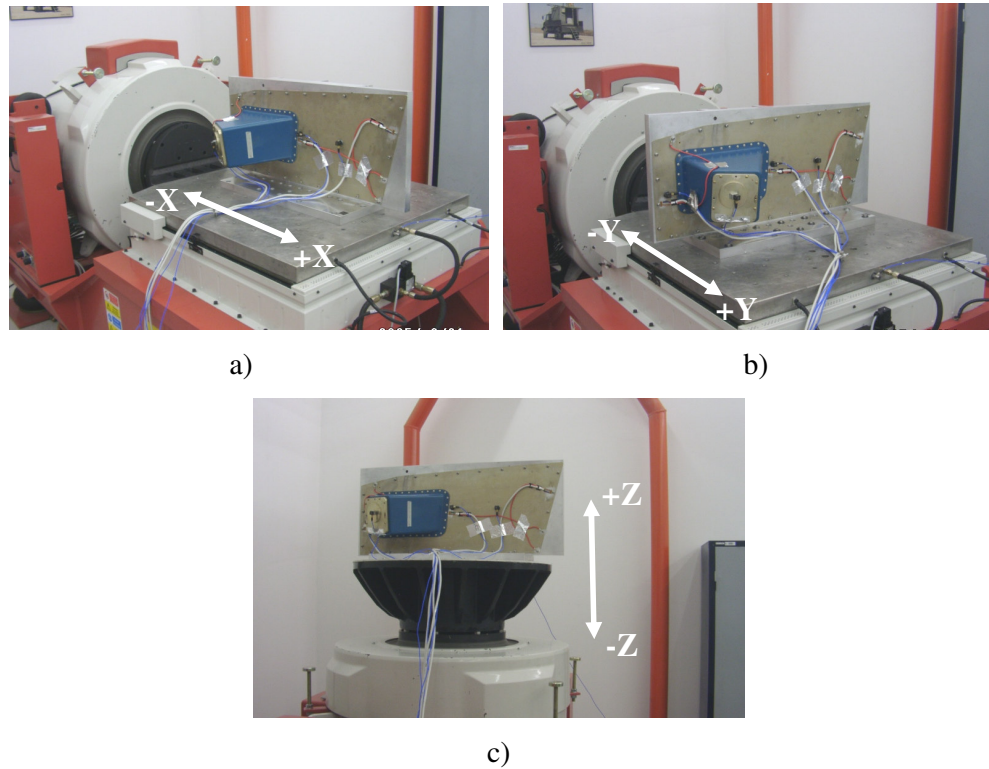


Figure 6.14: Excitation directions on the shaker, a) Longitudinal, b) Transverse, c) Vertical.

6.3. Failure Occurrence of MWS-Cowling Assembly by Resonance Tests

Operational life requirement of the assembly is satisfied by performing the endurance tests, as mentioned in the previous subchapter. However, the most critical region of the structure should be found out, in order to compare it with the finite element model.

Resonance tests are used for causing failures by continuously exciting the structure at its natural frequency, so that the failure is obtained as soon as possible. First natural frequency will be obtained by driving the shaker in transverse direction and with a constant amplitude random vibration profile (band

limited white noise) of 0-100 Hz. This bandwidth and direction of excitation is selected by considering the numerical modal analysis results.

An accelerometer is placed on the cowling at which first mode can be identified experimentally according to the numerically found first mode. The accelerometer is selected as 500g amplitude one, since relatively high g's can be obtained in resonance tests due to high response of structure at its resonance frequency. Location of the accelerometer is shown in Figure 6.15.

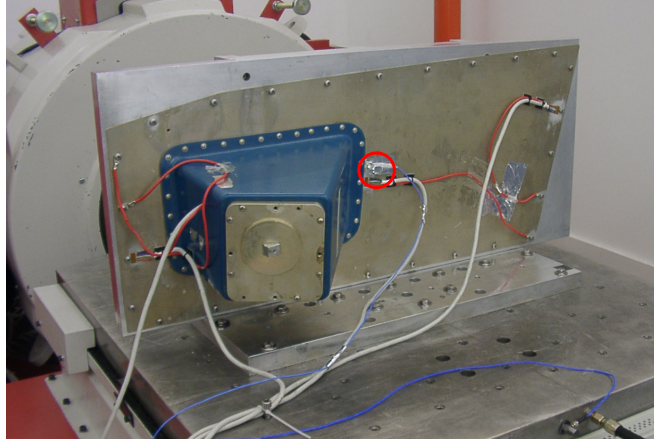


Figure 6.15: Position of the accelerometer placed on the cowling.

PSD graph of the accelerometer placed on the cowling under band limited white noise is given in Figure 6.16. The peak value corresponds to 77.5 Hz. This frequency is very close to what was found by numerical modal analysis (76 Hz). Thus, it can be taken as the first natural frequency of the assembly since the excitation is defined as band limited white noise. Therefore, the frequency found by this test will be used for the resonance tests.



Figure 6.16: PSD graph of the accelerometer on the cowling in transverse axis.

Resonance test in transverse direction is performed continuously until a physical failure is determined (5g amplitude). This value is selected intuitively so that failure will be obtained in a reasonable time. Detailed visual check is done in 5 minutes periods during the test. Resonance test continued for almost 6.5 hours, and a failure was observed at one of the holes used for connecting the cowling to the helicopter body. Crack location is shown in Figure 6.17 and Figure 6.18. The location of the crack is exactly at the same location as it was determined by the numerical fatigue analysis.



Figure 6.17: Front view of the crack location, a) Wide view, b) Closer view.

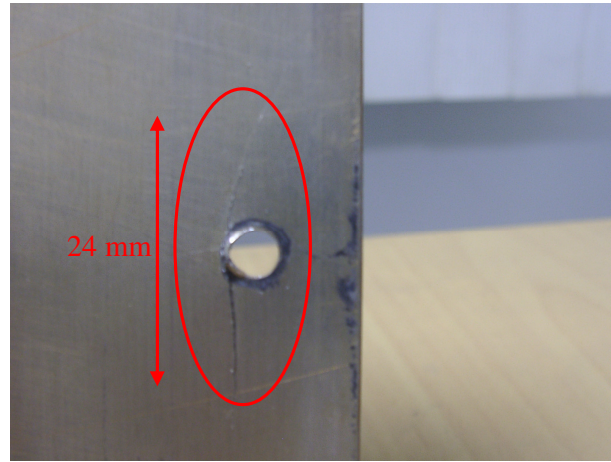


Figure 6.18: Back side view and size of the crack.

Resonance test is numerically simulated by using the previous finite element model of the assembly. Sine loading at 76 Hz with amplitude of 5g is applied in transverse axis to obtain the fatigue life of the structure if only resonance test is to be applied from the beginning. The critical location is determined as the same place in the previous analyses (Figure 6.19). In addition, the life is found out to be 5.22×10^4 seconds (14.5 hours), as given in Figure 6.20. Therefore, critical location is determined correctly and the life is obtained as an approximate result.

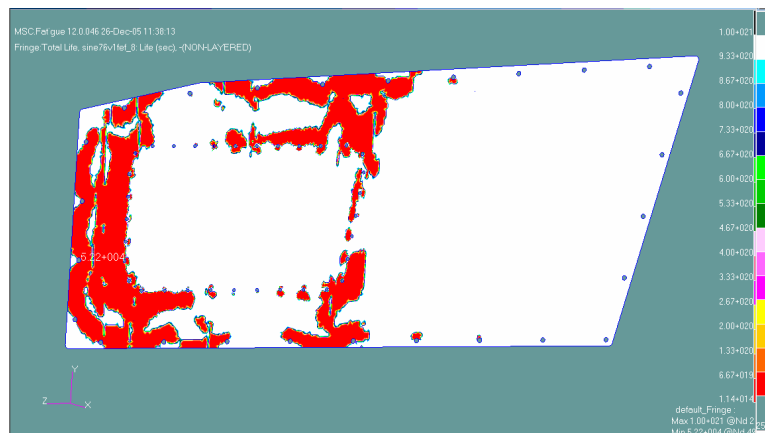


Figure 6.19: Life distribution on the cowling after resonance test simulation.

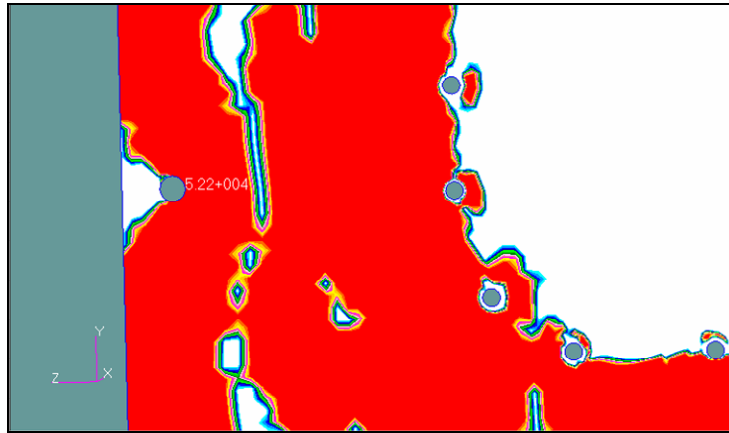


Figure 6.20: Critical location for the resonance test simulation.

6.4. Comparison of Numerical and Experimental Fatigue Analysis Results

Results of both numerical and experimental analysis show the same location as the most critical region on the structure from fatigue point of view. Minimum fatigue life location according to numerical analysis is shown in Figure 6.8, and fatigue crack location obtained in fatigue testing is shown in Figure 6.17.

The actual fatigue life in resonance testing is found to be 6.5 hrs as opposed to 14.5 hours from the numerical fatigue analysis. The discrepancy seems to be large. However, it should be noted that the resonance test has been applied to an already damage accumulated structure (although no macroscopic damage is observed) whereas numerical simulation assumes a perfectly undamaged material at the beginning. In addition, numerical analysis assumptions affect the life duration variance.

It is seen that numerical model of the structure is well representing the real assembly. This conclusion is a result of obtaining first natural frequency very close and correctly determining the fatigue fracture location.

It is appropriate to state basic assumptions and the shortcomings of two methods at this point.

- Mean stresses due to bolt tightening are not included in numerical analysis, since vibration fatigue does not take mean stresses into account.
- On the other hand, vibration tests are carried out axis by axis, not three axes simultaneously. In addition, resonance test is performed in one axis by considering the axis which would excite the first mode that is dominant.
- Another reason for selecting transverse (Y) axis as the resonance test vibration axis is having the maximum stress on the structure as a result of harmonic analysis.

Although the fatigue life obtained by numerical analysis is still questionable, critical location was determined correctly.

CHAPTER 7

EXPERIMENTAL STRESS ANALYSIS OF THE ASSEMBLY BY ACCELERATED LIFE TESTING

Analysis of the strain data collected by the rosettes will be discussed in this chapter. Strain data was measured under vibration levels for 1 hour-4 hours-100 hours-3000 hours accelerated profiles and 12000 hours operational vibration level during axis by axis testing, as mentioned in Chapter 6.2. All the steps for obtaining a useful stress result by raw strain data will be covered.

7.1 Experimental Data Processes and Fatigue Stress Analysis

At the beginning of the vibration tests, calibration and balancing of the strain gages are set when the assembly is at rest, such that each strain rosette has zero reading. After completing these settings, the assembly is rotated back to its original position. This is done for obtaining the mean strain values due to the static loading (gravity) of the MWS itself.

Raw gage readings of the rosette for the transverse axis (Y-axis) vibration under 1 hour accelerated vibration profile is given in Figure 7.1.

Before starting to analyze the raw data, a check of the random data is performed. Statistical quality of the random data is determined. After performing the necessary analyses, it is seen that the raw strain data has Gaussian characteristics. In addition, random and bias errors are calculated. Random error of 10.2% and bias error of 1.64% are determined. Brief information about measurement errors and outputs of the error study are given in APPENDIX E.

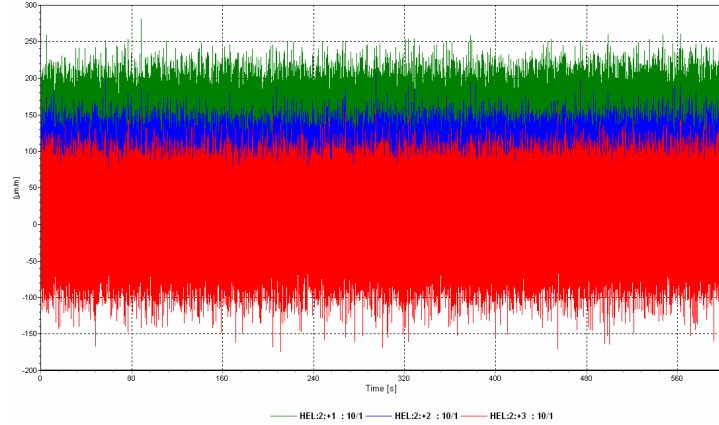


Figure 7.1: Raw strain data for each gage part of the analyzed rosette.

According to the numerical PSD analysis study discussed in APPENDIX F, addition of individual strain components at each axis vibration was in an error range of about 10%. It is concluded that the determined error is acceptable since there does not exist an available multiaxial shaker for the tests. Therefore, raw strain data for each axis is added for each gage of the rosette.

Summed strain data for the 1 hour accelerated life test is shown in Figure 7.2.

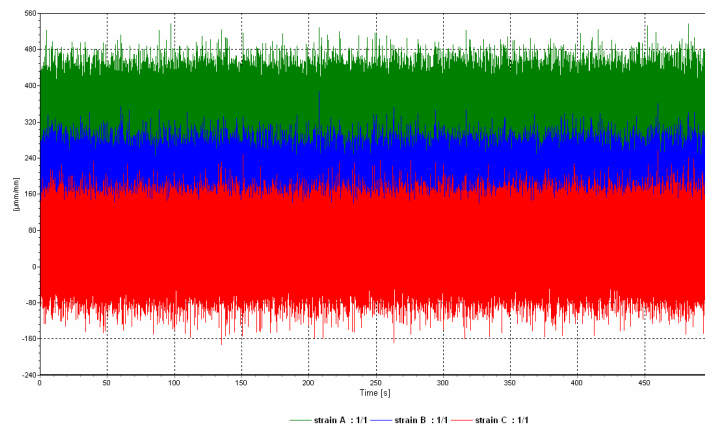


Figure 7.2: Combined strain data by summation.

Biaxiality check of the combined strain data that corresponds to 12000 hours operational life is performed to see the multiaxiality condition. In Figure 7.3, it is seen that the plot has proportional multiaxial case characteristics which means that the ratio of the principal stresses remain almost constant due to axis by axis simulation of the operational flight test.

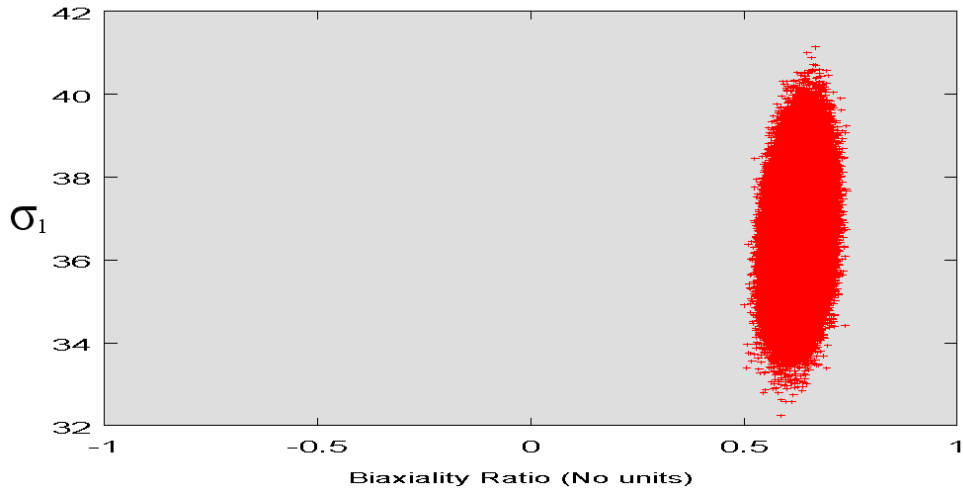


Figure 7.3: Principal stress vs. Biaxiality ratio plot of the combined strain data.

After obtaining the summed strain components for the gage readings, rosette analysis is performed. Brief information on experimental stress analysis and rosette calculations is given in APPENDIX H. Esam [24] software requires rosette type, cross sensitivities of the gages, poisson ratio and modulus of elasticity values for the rosette analysis. The analysis input sheet is seen in Figure 7.4. Analysis gives maximal principal stress, minimal principal stress, principal stress direction and absolute principal stress. Among the results of the analysis, absolute principal stress is the main parameter of interest as an output. It will be used for estimating a relation between the accelerated test duration and the stress level.

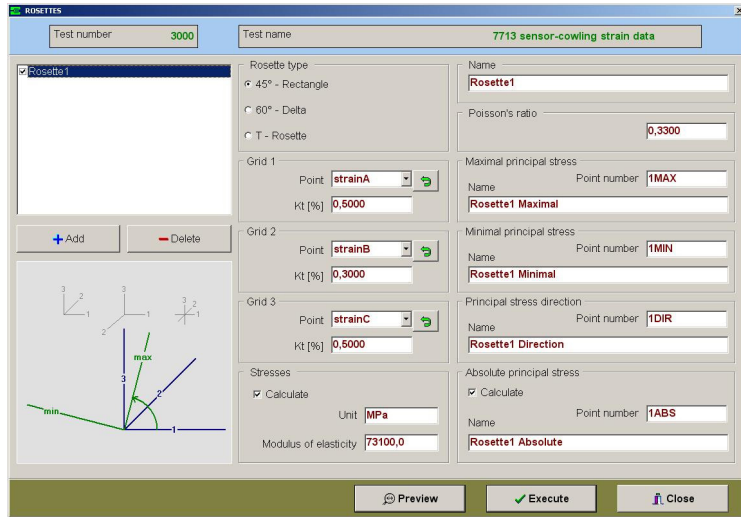


Figure 7.4: Rosette analysis input screen.

Residual stress due to riveting of 8.8 MPa is found in APPENDIX G. In order to take the residual stress into account, it should be included in the strain data. Therefore, a constant level of added strain is determined by trial and error. Rosette analysis is repeated for a number of times to obtain 8.8 MPa residual stress to be included in the absolute principal stress result. This is done due to the fact that the principal stress direction does not change much.

Finally, it is found out that adding $80\mu\text{mm}/\text{mm}$, to each gage reading, results in 8.8 MPa increase in the absolute principal stress. Figure 7.5 shows the shift in the strain data as a result of $80\mu\text{mm}/\text{mm}$ addition. In addition, absolute principal stress change for each accelerated test scenario due to strain addition is seen in Figure 7.6. By examining this graph, it can be easily noted that strain addition resulted in absolute principal stress variation of about 8.8 MPa, as it is desired.

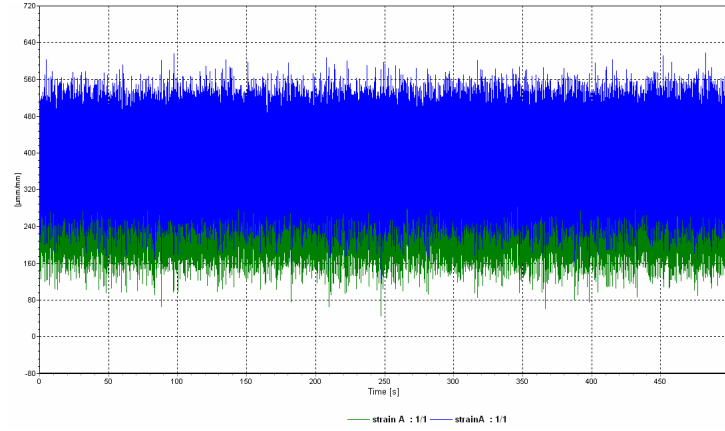


Figure 7.5: Strain reading comparison of before (green) and after (blue) adding $80 \mu\text{m}/\text{mm}$.

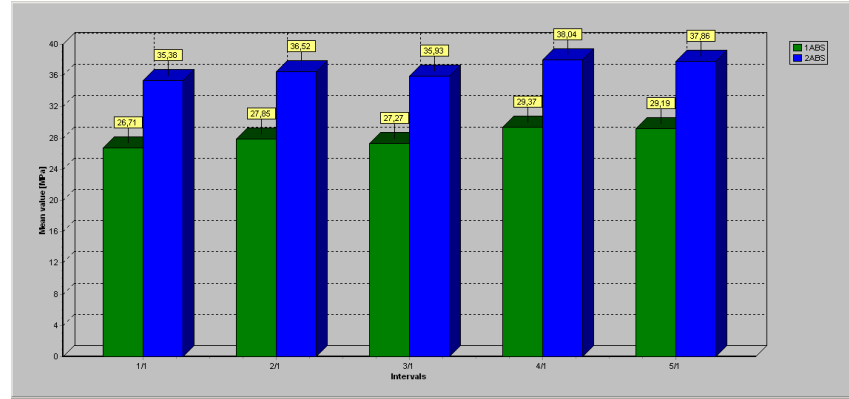


Figure 7.6: Mean of the absolute principal stresses for each test, before (green) and after (blue) including residual stresses due to riveting.

Rainflow cycle counting of the absolute principal stress data is performed. As it is expected for random type of loading cases, arrow head type of profile is obtained. In addition, mean and alternating stress distribution on the component can be seen by inspecting the rainflow plot. Therefore, stress distributions on the analyzed location can be seen by comparing the rainflow plots of different test scenarios, such as 1 hour and 100 hours accelerated life testing. In Figure 7.7 and Figure 7.8, rainflow counting plots of 1 hour and 100 hours accelerated vibration tests are given.

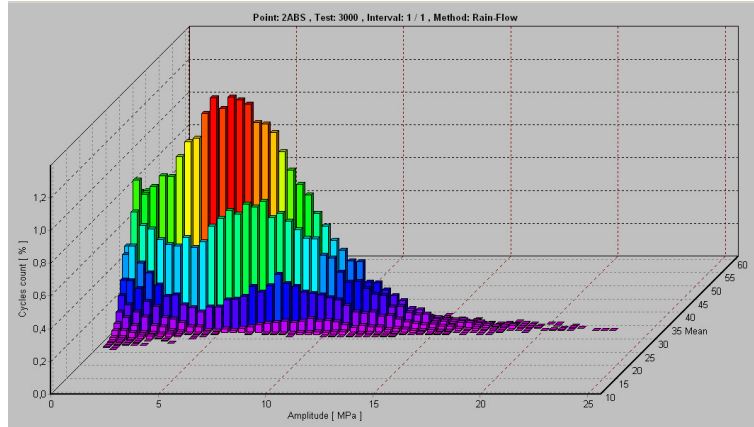


Figure 7.7: Rainflow counting result of 1 hour accelerated test.

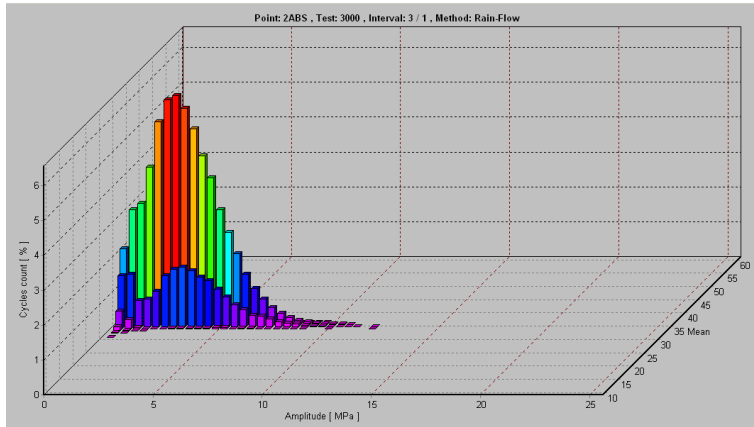


Figure 7.8: Rainflow counting result of 100 hours accelerated test.

Examining the above plots, it is seen that variation of absolute principal stress is more spread out in the 1 hour accelerated test. This is a result of response characteristics due to higher vibration levels. On the other hand, percent occurrence of each stress component is higher in 100 hours accelerated test.

An equivalent alternating stress amplitude can be computed by using the below equation (7.1) with the individual amplitudes obtained by rainflow cycle counting. Esam software automatically applies this equation to the counted

quantities. It uses an "m" value of 6. Application of m=6 value is a common selection for stress analysis cases [24].

$$A = \sqrt[m]{\frac{1}{\sum C_i} \cdot \sum (A_i^m \cdot C_i)} \quad (7.1)$$

where,

A : Equivalent amplitude

A_i : Individual amplitudes

C_i : Number of cycles of individual stresses

m : Averaging exponent

Therefore, equivalent stress amplitude of each test is computed. Equivalent mean is already estimated by taking the means of each random data oscillation. Consequently, pure random data is approximated as a constant amplitude alternating stress which has a non-zero mean.

Esam software output screen showing the mean and alternating equivalent stresses for 1 hour accelerated test is shown in Figure 7.9.

Mean and alternating stress representations of each test scenario is given in Figure 7.10. It is seen that mean stress stays almost constant and alternating stress decreases from 1 hour accelerated test to 12000 hours accelerated test (left to right).

Results	Minimum	10,90409	Mean	35,38004	Maximum	56,68028
	Classes	515	Cycles	71189	Half-cycles	9
			<input type="text" value="Equivalent amplitude 9,107814"/> $A = \sqrt[m]{\frac{1}{\sum C_i} \cdot \sum (A_i^m \cdot C_i)}$ <input type="text" value="m = 6"/> <input type="button" value="Apply"/>			

Figure 7.9: Mean and alternating equivalent stresses for 1 hour accelerated test.

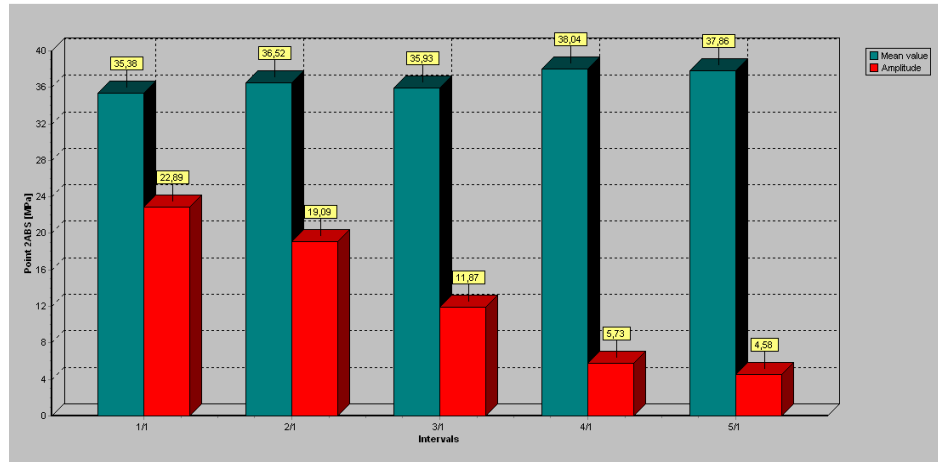


Figure 7.10: Distribution of mean and alternating stresses.

However, it is more convenient to have a single alternating stress with zero mean. Therefore, a final equivalent stress value is calculated by using Soderberg Equation, as given in APPENDIX-A. The calculation is done for all of the analysis results of 1 hour, 4 hours, 100 hours, 3000 hours and 12000 hours accelerated tests.

In other words, σ_e is calculated by using the below equation (Equation 7.2) with the single alternating (σ_a), single mean stress (σ_m) and material strength constants (yield strength $S_y = 345$ MPa, fatigue strength $S_e = 138$ MPa).

$$\frac{\sigma_m}{S_y} + \frac{\sigma_a}{S_e} = 1 \quad (7.2)$$

The finalized equivalent stresses are tabulated in Table 7.1. It is seen that equivalent stress amplitude decreases as the accelerated test duration increases.

Table 7.1: Equivalent alternating stress results for test scenarios.

Accelerated Life Test (t₁, t₂) [hour]	Equivalent Stress Amplitude (S₁, S₂) [MPa]
1	10.151
4	8.231
100	5.347
3000	2.754
12000	2.123

7.2. Obtaining Accelerated Life Testing Time Relation

After having converted the random stress history to a set of equivalent stresses for all accelerated test scenarios, the aim of the study at this point, is to determine a relation between stresses and test durations.

Therefore, a relationship is obtained by using the equivalent alternating stresses.

$$\left(\frac{\sigma_1}{\sigma_2} \right)^c = \frac{t_2}{t_1} \quad (7.3)$$

where,

σ_1 : Real time equivalent alternating stress (MPa)

σ_2 : Laboratory test equivalent alternating stress (MPa)

c : Coefficient to be determined

In order to determine the coefficient “c”, test durations and pre-determined equivalent alternating stresses are used in pairs with equation 7.3.

The distribution of coefficient “c” that is obtained by cross relating the equivalent alternating stresses and corresponding accelerated test durations is given in Table 7.2.

Table 7.2: Coefficient “c” table according to the entire test scenario pairs.

Accelerated Life Test	1 hour	4 hours	100 hours	3000 hours	12000 hours
1 hour	x	6.613	7.184	6.137	6.003
4 hours	6.613	x	7.461	6.046	5.908
100 hours	7.184	7.461	x	5.125	5.183
3000 hours	6.137	6.046	5.125	x	5.329
12000 hours	6.003	5.908	5.183	5.329	x

It is seen that coefficient “c” varies in the range of 5 to 7.5, having an arithmetical average of 6.25 that can be used as a structural stress parameter.

The value of “c” is closer to 5 when operational profile is accelerated with higher ratios and it is closer to 7.5 when operational profile is accelerated with lower ratios.

The mechanism behind the accelerated life testing is to accelerate the possible failures while keeping the total damage constant. The main logic of the proposed relation is similar to the material S-N diagrams. The value “b” of the S-N diagram equation, $N\sigma^b = C$, for aluminum alloys vary and the values of 6.4 or 9.0 is suggested for most of the applications in the literature according to the type of fatigue test [19].

- b= 5.6, for axial loading
- b= 6.4, for rotating beam
- b= 8.9, for bending beam

However, the coefficient “c” that is proposed in this study is experimentally obtained by component testing and it contains operational loading data and geometry of the design. The corresponding equation (Equation 7.3) can be used with accelerated life test limitations beyond that failure may occur. In classical application of standards, Equation 4.7 can be used without any accelerated time

limitations and it can not prevent the loading level to exceed the yield strength of the material.

In addition, the most appropriate accelerated life test duration can be estimated by knowing the experimental “c” value of a structure. Since the equivalent alternating stresses in the study are low due to lightweight composite sensor and its location on the helicopter, optimization of the test duration is not necessary for this study. However, there are many critical conditions for the structures used in the industry, especially in aerospace platforms where safety factors are set relatively lower due to weight limitations. This makes accelerated life test durations critical.

CHAPTER 8

DISCUSSION AND CONCLUSION

Vibration induced stress and fatigue analysis of missile warning sensor (MWS) and cowling assembly of AH-1P Cobra helicopter has been performed by using accelerated life testing approach in this study. Experimental, numerical and analytical methods are used wherever appropriate in order to complete the analyses in the product design cycle.

It is difficult to analyze structures under broad band random loading. The reason is the probability of having natural frequencies coincident with excitation frequencies. In this case, the response of the structure is controlled by the mode shapes. Therefore, frequency domain approaches should be preferred instead of time domain fatigue approaches. Vibration fatigue method is a technique used for such cases in which multiaxial PSD is the loading. Triaxial PSD levels at the region of interest are obtained by operational flight tests.

Operational flight tests have been performed for triaxial acceleration data acquisition at the MWS integration point. An important consideration is that the vibration level at the location should not change much when the actual unit is mounted. In other words, it is initially considered that the dynamic characteristics of the mounting region remain almost constant after integration of the equipment. This assumption can be verified by taking measurements at the same location at the end of the integration and comparing them with the previous ones. The vibration profiles can be updated, if a change in vibration characteristics is observed after comparison. Since this study has been done as a part of an ongoing ASELSAN project, comparison analysis will be considered as a future study for the time being.

Numerical fatigue analysis of the MWS-cowling assembly has been performed. According to the results of numerical fatigue analysis, the assembly has a fatigue life of 2.32×10^{16} seconds (6.44×10^{12} hours). The most critical location corresponds to a boundary hole. In addition, resonance test simulation resulted in a total life of 5.22×10^4 seconds (14.5 hours) at the same location. Vibration fatigue technique determines the critical location efficiently. However, numerical value of the fatigue life may not be as correct for the boundaries, since vibration fatigue method neglects the elastic and plastic deformations as a result of residual stresses created by bolts and rivets. In other words, mean stresses are not taken into account in this method. Therefore, determined critical location can be used as the point of focus for the experimental analyses. The results can be optimized by performing mesh sensitivity analysis to reduce the stress concentrations that can be a result of coarse mesh. In addition, increasing the number of frequency steps increase the response resolution.

Experimental fatigue analysis has been performed to check whether the prototype indeed satisfies the 12000 hours operational life. Indeed, the assembly satisfies the operational life requirements specified by the customer and the standards. Fatigue testing of the assembly has been performed axis by axis and no failure was seen. Furthermore, resonance testing has been done by exciting the first mode shape of the assembly. A crack was observed during the resonance tests at the same location it was determined by the numerical fatigue analysis. The total test duration was approximately 38000 hours operational life equivalent fatigue test and 6 hours of resonance test. Hence, it is concluded that critical location can be effectively determined by numerical fatigue analysis, even at the boundaries, if the structure is modeled correctly.

In order to avoid the axis by axis versus multiaxial vibration tests assumption 6-DOF vibration test equipment should be used. Cross correlations between each axis and the moments are perfectly transferred to the structure by 6-DOF test equipment. However, this kind of vibration test equipment is not very commonly used in the industry yet.

According to military standards and ITOP, maximum exaggeration level of 3dB is recommended for the real time operational spectrum. The exaggeration equation given in these standards can be used, unless testing is possible. However, material, loading and design consideration effects are not included in this equation. It is known that nonlinearities due to loading and geometry have significant role on the stress levels. Therefore, it is more appropriate to test the actual prototype, determine the equivalent stress level and evaluate the accelerated test duration by the equation proposed in this study.

A relationship between equivalent alternating stresses and accelerated test durations has been brought up in this study. When the correlation coefficient “c” values determined for each test scenario pairs are inspected, it is easily seen that “c” values fall between 5.0 and 7.5, with an average of 6.25. This value is considered to be acceptable, as an order with the similar parameter “b”, since it falls in the range found in the literature. Coefficient “c” also includes effects of mean and residual stresses on the cowling, although they are not high in this study. It is known that the curve on the S-N diagram is a representation of stress values and the number of cycles at that stress level for total damage value of unity. The coefficient “c” that is proposed in this study is experimentally obtained by component testing, it contains operational loading data and geometry of the design, whereas, “b” is obtained by material S-N diagrams.

Since the correct relationship between the equivalent alternating stresses and accelerated life testing durations have been determined, appropriate accelerated test duration can be evaluated by avoiding the maximum stress level to reach or exceed the yield limit. It has been found out that the stress levels are not close to the yield limit of the material, even for 1 hour accelerated test, in this study. However, the approach or the methodology used in this study shall be applied on electronic equipments or relatively small structures which may be more critical in stress levels.

REFERENCES

- [1] Lalanne, C., *Mechanical Vibration & Shock, Fatigue Damage*, Vol IV, Taylor & Francis Books, London, 2002.
- [2] LMS Mission Synthesis Release 3.5.D Software Manual and Training Notes, LMS International, Belgium, 2003.
- [3] Lagoda, T., Macha, E., Pawliczek, R., “The Influence of the Mean Stress on Fatigue Life of 10HNAP Steel under Random Loading”, International Journal of Fatigue, Vol.23, pp.283-291, 2001.
- [4] Szlowinski, M. P., Farris, T. N., “Linking Riveting Process Parameters to The Fatigue Performance of Riveted Aircraft Structures”, Journal of Aircraft, 2000, Vol.37 No: 1, pp.130-137.
- [5] Byrne, T.P., Morandin, G.D., “A Multiaxial Fatigue Cycle Counting Technique Based on the Rainflow Method”, ASME, PVP Vol.370, 1998.
- [6] Carpinteri, A., Macha, E., Brighenti, R., Spagnoli, A., “Expected Principal Stress Directions under Multiaxial Loading”, International Journal of Fatigue, Vol.21, pp.83-96, 1999.
- [7] Çelik, M., “Kaideye Monteli Stinger Sisteminin Taret Deneysel Yorulma Analizi” SAVTEK-2002 Savunma Teknolojileri Kongresi, Orta Doğu Teknik Üniversitesi, Ankara, 2002, 321-332.
- [8] Colombi, P., Dolinski, K., “Fatigue Lifetime of Welded Joints under Random Loading: Rainflow Cycle vs. Cycle Sequence Method”, Probabilistic Engineering Mechanics, Vol.16, pp.61-71, 2001.
- [9] Winter, P.W., Macinnes, D.A., “Fatigue under Variable Amplitude Loading: A New Approach”, ASME, OMAE Vol.2, 1993.
- [10]Holm, S., de Mare, J., “A Simple Model for Fatigue Life”, IEEE Transactions on Reliability, Vol.37, No.3, 1988.
- [11]Pitoiset, X., Preumont, A., Kernilis, A., “Tools for a Multiaxial Fatigue Analysis of Structures Submitted to Random Vibrations”, European Conference on Spacecraft Structures Materials and Mechanical Testing, 1998.
- [12]Fu, T.T., Cebon, D., “Predicting Fatigue Lives for Bi-modal Stress Spectral Densities”, International Journal of Fatigue, Vol.22, pp.11-21, 2000.

- [13] Shang, G., Wang, K., Li, M., Yao, W., “Local Stress-Strain Field Intensity Approach to Fatigue Life Prediction under Random Cyclic Loading”, International Journal of Fatigue, Vol.23, pp.903-910, 2001.
- [14] Kuntay, A., İpek, G., Güngör, S., “Accelerated Life Test Development for Engine Mounts”, SAE International, 2003.
- [15] Hieber, G., “Use and Abuse of Test Time Exaggeration Factors”, www.ttiedu.com, June 2005.
- [16] nCode Training Notes, “Integrated Durability Management”, December 2004.
- [17] MSC Fatigue Version 2003 User’s Manual, MSC Software Inc., USA, 2003.
- [18] Aykan, M., “Vibration Fatigue Analysis of Equipments used in Aerospace”, M.S. Thesis, Middle East Technical University, Ankara, 2005.
- [19] Lalanne, C., *Mechanical Environment Test Specification Development Method*, Le Barp, France.
- [20] MIL-STD-810F, “Environmental Engineering Considerations and Laboratory Tests”, Department of Defense Test Method Standard, USA, 2000.
- [21] International Test Operations Procedure (ITOP) 1-1-050, Development of Laboratory Vibration Test Schedules, 1993.
- [22] MIL-STD-810E, “Environmental Test Methods and Engineering Guidelines”, Department of Defense Test Method Standard, USA, 1989.
- [23] PCB Product Catalog, Shock and Vibration Sensors Division, USA, 1999.
- [24] Traveller Plus and ESAM Software Manual, Measurements Group Inc., Munich, 2000.
- [25] Steinberg, D.S., *Vibration Analysis for Electronic Equipment*, Second edition, John Wiley&Sons, USA, 1988.
- [26] ANSYS Release 8.1 User’s Manual, ANSYS Inc., USA, 2003.
- [27] Catalogs for Strain Gages Accessories and Instruments, Measurements Group-Vishay, 2005.
- [28] Hexagon SR1+ module, Bolted Joint Calculation, version 9.42, 1999.
- [29] LDS V895-440 HBT 900C Model Vibration Shaker User’ Manual, Ling Dynamics Inc., England, 2004.

- [30] Shigley, J. E., *Mechanical Engineering Design*, First Metric Edition, McGraw-Hill, 1986.
- [31] Dieck, R.H., *Measurement Uncertainty*, Instrument Society of America, USA, 1992.
- [32] Çelik, M., Ozsoy, S., "AH-1P Helikopteri Operasyonel Titreşim Profili Oluşturma Testleri", Teknik Rapor, ASELSAN, 2004.
- [33] MSC Marc Version 2003 User's Manual, MSC Software Inc., USA, 2003.
- [34] Kuru, D., Çermikli, H., Lafçı, A., "Kompozit Yapı Üretim Teknikleri Değerlendirme Raporu", Teknik Rapor, ASELSAN, 2004.
- [35] Fibreglass Composites, "Design Data", Fibreglass Limited Reinforcements Division, England.
- [36] MatWeb, "The Online Materials Information Resource", www.matweb.com, July 2005.
- [37] Hexagon WST1 module, Material Database, version 6.4, 1999.
- [38] Vaughan, J., *Application of B&K Equipment to Strain Measurements*, B&K, Denmark, 1975.

APPENDIX-A

EFFECT OF MEAN STRESS ON FATIGUE LIFE AND RAINFLOW CYCLE COUNTING METHOD

While using the S-N graphs, effect of mean stress should be taken into account. Level of the mean stress in a fluctuating stress history is very significant (Figure A.1). Endurance of structures decreases with increasing positive (tensile) mean stress. Whereas, negative mean stress (compressive) increases the fatigue life of the structures.

There are several methods developed to take the mean stress effect into account. Most common ones of these methods are Goodman, Gerber and Soderberg approaches. Soderberg approach is the most conservative one among these methods. Each method has its own criteria and the safety curves represented according to these criterions can be seen in Figure A.2.

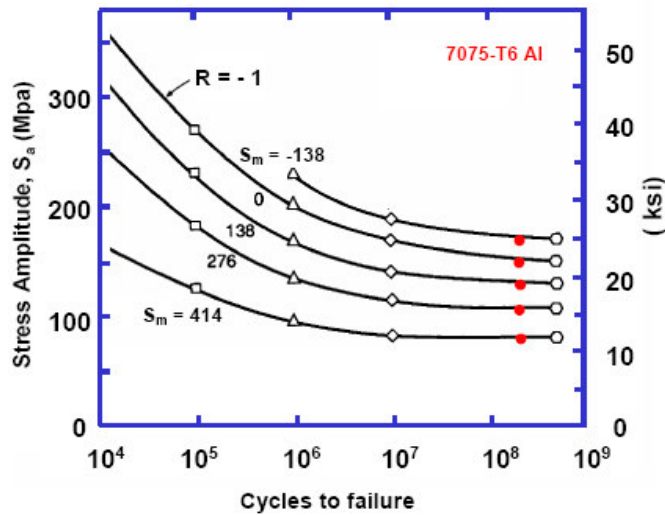


Figure A.1: Effect of mean stress on fatigue life [16].

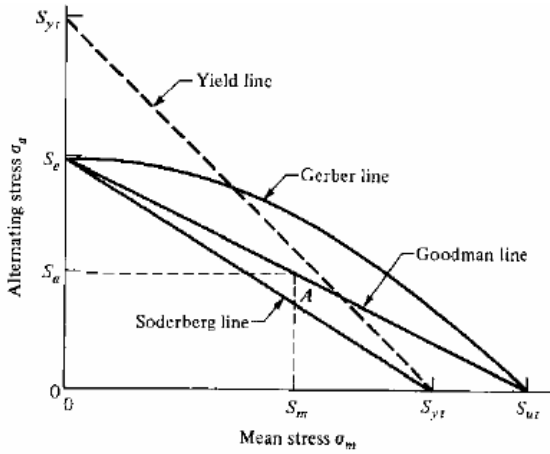


Figure A.2: Boundary curves of different mean stress correction methods [30].

The equations of the mean stress correction methods shown in Figure A.2 are stated below.

Goodman's model:

$$S_a' = S_a / (1 - (S_m / S_{ut})) \quad (\text{A.1})$$

Soderberg's model:

$$S_a' = S_a / (1 - (S_m / S_{yt})) \quad (\text{A.2})$$

Gerber's model:

$$S_a' = S_a / (1 - (S_m / S_{ut})^2) \quad (\text{A.3})$$

where;

S_a' : Equivalent alternating stress

S_a : Alternating stress

S_m : Mean stress

S_{ut} : Ultimate tensile strength

S_{yt} : Tensile yield strength

Having covered the above approaches, damage accumulated in structures can be introduced. Fatigue failure is a cumulative failure as a result of damage created by loading. Considering a consecutive loading (Figure A.3), each individual loading has a contribution on the total damage on the structure.

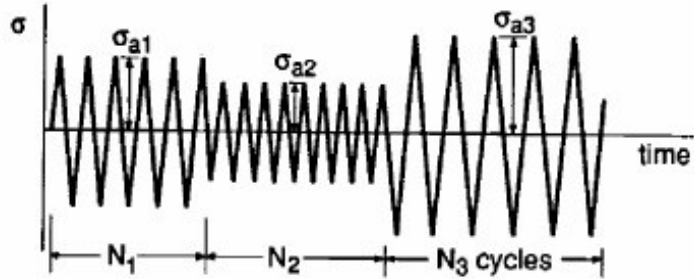


Figure A.3: Consecutive loading experienced by a structure.

Among the several cumulative damage fatigue theories known, the most commonly used and best known is the one suggested by Palmgren and later independently by Miner. The Palmgren-Miner hypothesis is that the fatigue damage caused at a stress level is proportional to the number of cycles applied at that stress level divided by the total number of cycles required to experience failure at the same level. This damage is usually referred as the cycle ratio or cumulative damage ratio. If the repeated loads are continued at the same level until failure occurs, the cycle ratio will equal to one. On the other hand, when fatigue loading involves many levels of stress amplitude, the total damage is a sum of different cycle ratios and failure still occurs when the summation equals to one.

Below is the formula which represents the Palmgren-Miner rule.

$$\sum_{i=1}^k \frac{n_i}{N_i} = 1 \quad (\text{A.4})$$

where;

n : The number of stress cycles applied at a fixed stress amplitude

N : The number of cycles the material can withstand at applied fixed stress amplitude

k : The number of stress cycle blocks with different amplitudes and/or means

The signal measured, in general a random stress $\sigma(t)$, is not always made up of a peak alone between two passages by zero. On the other hand, several peaks often appear which makes difficult the determination of the number of cycles absorbed by the structure.

Therefore, several methods of counting were proposed for random signals. The most common ones are listed below:

- Peak count,
- Range count,
- Range-mean count,
- Racetrack method,
- Level crossing count,
- Fatiguemeter count,
- Rainflow cycle count.

All of these methods carry out the fatigue damage evaluation in three steps:

- Counting of the cycles,
- Choice of a relation cycle – generated damage,
- Summation of the damage generated by each cycle.

Among the above methods, Rainflow cycle counting method will be explained briefly, since it will be used in this study due to its efficiency in fatigue calculations. The method provides all the necessary information for damage evaluations such as mean stress, alternating stress and number of cycles.

Rainflow cycle counting method was initially proposed by M. Matsuiski and T. Endo to count the cycles or the half cycles of strain-time signals. The Rainflow counting algorithm searches the time signal for cycles having the same amplitude and mean, and then groups these into pairs. Typical Rainflow counting output presentation is given in Figure A.4.

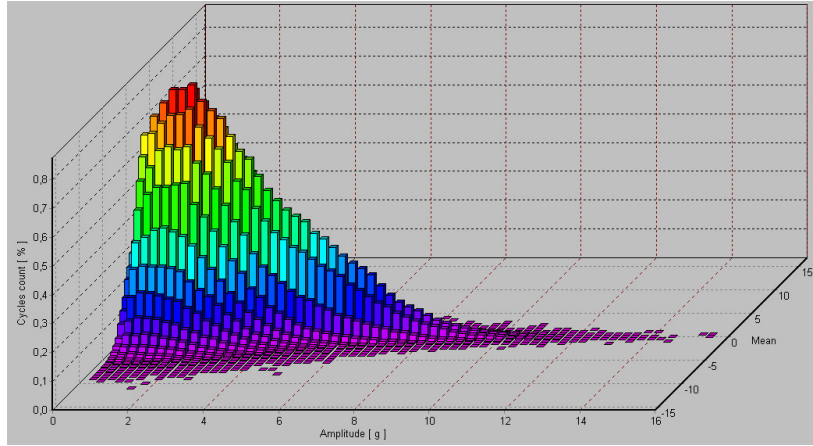


Figure A.4: Rainflow counting graphical presentation.

A simple procedure for Rainflow counting is given below:

- Extract peaks and gutters from the time signal so that all points between adjacent peaks and gutters are discarded.
- Arrange the signal so that the beginning, and end, of the sequence have the same level. An additional point can be created at the end of the signal to match the beginning.
- Determine the highest peak and reorder the signal so that this becomes the beginning and the end. The beginning and end of the original signal have to be joined together.
- Start at the beginning of the sequence and pick consecutive sets of 4 peaks and gutters. Apply a rule that states, if the second segment is shorter (vertically) than the first, and the third is longer than the second, the middle segment can be extracted and recorded as a Rainflow cycle.

- If no cycle is counted then a check is made on the next set of 4 peaks, i.e. peaks 2 to 5, and so on until a Rainflow cycle is counted. Every time a Rainflow cycle is counted the procedure is started from the beginning of the sequence again.

Visual explanation of Rainflow cycle counting method procedure is shown in Figure A.5.

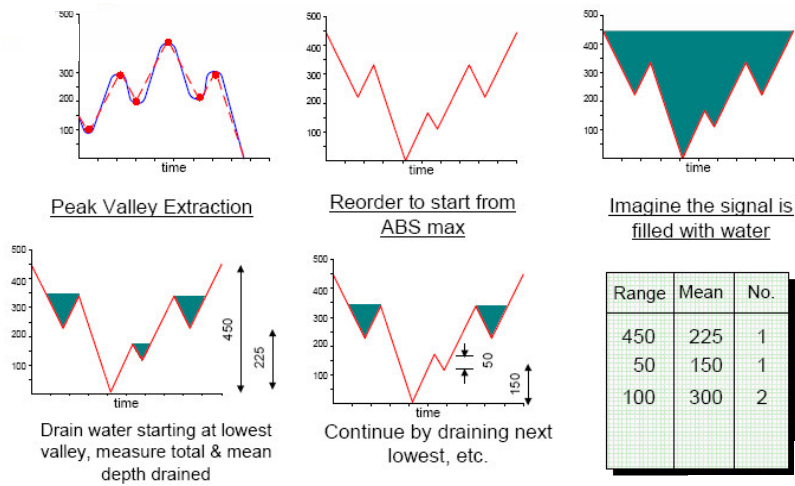


Figure A.5: Application of Rainflow cycle counting method [16].

APPENDIX-B

OPERATIONAL FLIGHT PROFILE

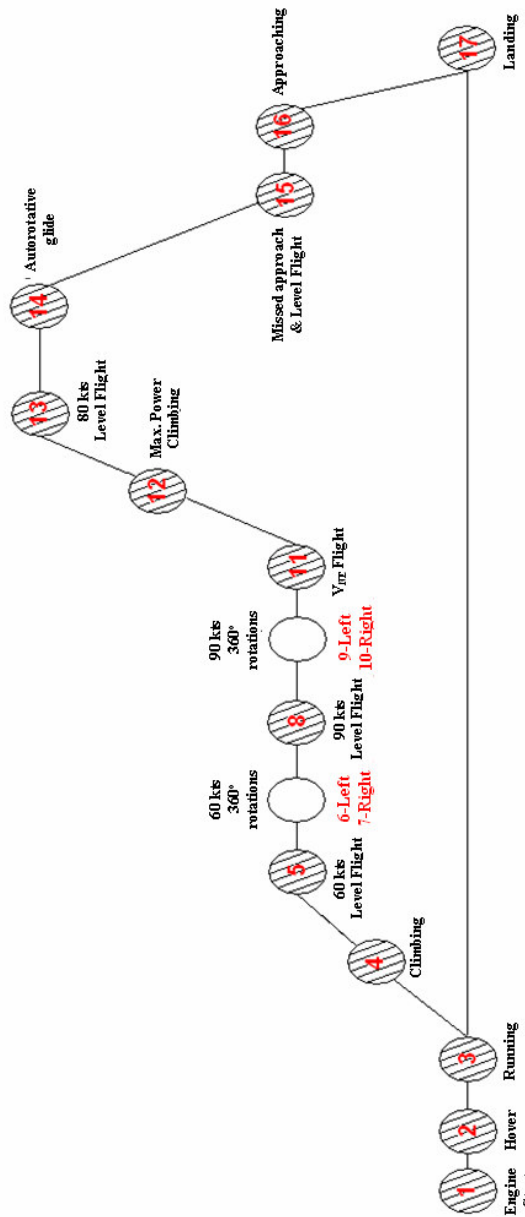


Figure B.1: Flight profile followed during operational tests [32].

APPENDIX-C

PRINCIPLES OF PIEZOELECTRIC SENSORS

The piezoelectric effect, discovered in 1880 by Pierre and Jacques Curie, remained a mere curiosity until the 1940s. The property of certain crystals to exhibit electrical charges under mechanical loading was of no practical use until very high input impedance amplifiers enabled engineers to amplify the signals produced by these crystals. In the 1950s, electrometer tubes of sufficient quality became available and the piezoelectric effect was commercialized.

Piezoelectric accelerometers rely on the piezoelectric effect of quartz or ceramic crystals to generate an electrical output that is proportional to applied acceleration. The piezoelectric effect produces an opposed accumulation of charged particles on the crystal. This charge is proportional to the applied force or stress. A force applied to a quartz crystal lattice structure alters alignment of positive and negative ions, which results in an accumulation of these charged ions on opposed surfaces. These charged ions accumulate on an electrode that is ultimately conditioned by transistor microelectronics.

An internal view of a uniaxial ICP (Integrated Circuit Piezoelectric) accelerometer is given in Figure C.1.

These devices operate well over a wide frequency range, but they are not generally well suited to low-frequency applications. In addition, they can only sense dynamic quantities. Piezoelectric accelerometers are not suitable for static acceleration measurements, such as gravity, due to the working principle.

Typical acquisition set up for ICP accelerometers is shown in Figure C.2.

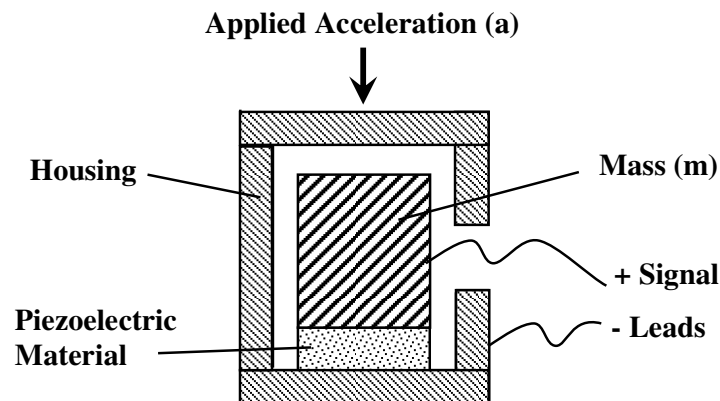


Figure C.1: Internal view of ICP accelerometers.

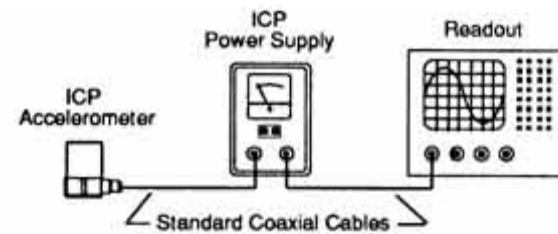
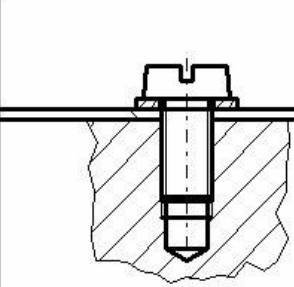


Figure C.2: ICP laboratory set up.

APPENDIX-D

BOLT ANALYSIS SHEET

DIN84 - M6 x 10 - 10.9																																																															
																																																															
<table border="1"> <thead> <tr> <th>i [mm]</th> <th>da [mm]</th> <th>di [mm]</th> <th>l [mm]</th> <th>material</th> </tr> </thead> <tbody> <tr> <td>1</td> <td>10.0</td> <td>5.3</td> <td>1.0</td> <td>Stainless steels,hardened</td> </tr> <tr> <td>2</td> <td>64.0</td> <td>5.0</td> <td>1.0</td> <td>Al 6061-T6</td> </tr> </tbody> </table>				i [mm]	da [mm]	di [mm]	l [mm]	material	1	10.0	5.3	1.0	Stainless steels,hardened	2	64.0	5.0	1.0	Al 6061-T6																																													
i [mm]	da [mm]	di [mm]	l [mm]	material																																																											
1	10.0	5.3	1.0	Stainless steels,hardened																																																											
2	64.0	5.0	1.0	Al 6061-T6																																																											
<table border="1"> <thead> <tr> <th colspan="3">termin. bolted joint (ESV)</th> </tr> </thead> <tbody> <tr> <td colspan="3">material : Al 6061-T6</td> </tr> <tr> <td>m</td> <td>mm</td> <td>8.0</td> </tr> <tr> <td>m min Dose</td> <td>mm</td> <td>6.3</td> </tr> <tr> <td>m min VDI2230</td> <td>mm</td> <td>8.0</td> </tr> </tbody> </table>				termin. bolted joint (ESV)			material : Al 6061-T6			m	mm	8.0	m min Dose	mm	6.3	m min VDI2230	mm	8.0																																													
termin. bolted joint (ESV)																																																															
material : Al 6061-T6																																																															
m	mm	8.0																																																													
m min Dose	mm	6.3																																																													
m min VDI2230	mm	8.0																																																													
<table border="1"> <tr><td></td></tr> <tr><td></td></tr> <tr><td></td></tr> <tr><td></td></tr> </table>																																																															
<p style="transform: rotate(-90deg); transform-origin: left top;">This document and giving it to other and the use intention of the contents, if not, are prohibited with- out authority. Offenders are liable to the payment of damages. All rights are reserved in the event of the grant of the registration of utility model or design.</p>	LOAD ($T=20^{\circ}\text{C}$)		<table border="1"> <thead> <tr> <th colspan="2">ASSEMBLY (Bolt driven)</th> <th>FRICTION</th> <th>min</th> <th>max</th> </tr> </thead> <tbody> <tr> <td>nue Rp</td> <td></td> <td>0.52</td> <td>μG</td> <td>0.180</td> </tr> <tr> <td>alpha A</td> <td></td> <td>2.00</td> <td>μK</td> <td>0.180</td> </tr> <tr> <td>MA max/min</td> <td>Nm</td> <td>4 / 2</td> <td>μTr</td> <td>0.950</td> </tr> <tr> <td>alpha max/min</td> <td>deg</td> <td>4.843 / 2.422</td> <td>K</td> <td>0.239</td> </tr> <tr> <td colspan="5">FACTORS OF SAFETY ($T=20^{\circ}\text{C}$)</td> </tr> <tr> <td>safety against loosening</td> <td></td> <td>FM,max/Fmmax,req</td> <td colspan="2">172.78</td> </tr> <tr> <td>safety yield point red.B</td> <td></td> <td>SF = Rp/Sig.redB</td> <td colspan="2">2.52</td> </tr> <tr> <td>safety plate surface pressure</td> <td></td> <td>Sp=pG/pmax</td> <td colspan="2">4.86</td> </tr> <tr> <td>safety against slipping due to FQ</td> <td></td> <td>SG=Fkmin/FkQreq</td> <td colspan="2">525.72</td> </tr> <tr> <td>thread strip safety at Rp</td> <td></td> <td>m/m min.</td> <td colspan="2">1.27</td> </tr> <tr> <td>thread strip safety at FM,max+FSA</td> <td></td> <td>tau Rp / tau B,M</td> <td colspan="2">3.67</td> </tr> </tbody> </table>	ASSEMBLY (Bolt driven)		FRICTION	min	max	nue Rp		0.52	μG	0.180	alpha A		2.00	μK	0.180	MA max/min	Nm	4 / 2	μTr	0.950	alpha max/min	deg	4.843 / 2.422	K	0.239	FACTORS OF SAFETY ($T=20^{\circ}\text{C}$)					safety against loosening		FM,max/Fmmax,req	172.78		safety yield point red.B		SF = Rp/Sig.redB	2.52		safety plate surface pressure		Sp=pG/pmax	4.86		safety against slipping due to FQ		SG=Fkmin/FkQreq	525.72		thread strip safety at Rp		m/m min.	1.27		thread strip safety at FM,max+FSA		tau Rp / tau B,M	3.67	
	ASSEMBLY (Bolt driven)			FRICTION	min	max																																																									
	nue Rp			0.52	μG	0.180																																																									
	alpha A			2.00	μK	0.180																																																									
	MA max/min	Nm		4 / 2	μTr	0.950																																																									
	alpha max/min	deg		4.843 / 2.422	K	0.239																																																									
	FACTORS OF SAFETY ($T=20^{\circ}\text{C}$)																																																														
	safety against loosening			FM,max/Fmmax,req	172.78																																																										
	safety yield point red.B			SF = Rp/Sig.redB	2.52																																																										
	safety plate surface pressure			Sp=pG/pmax	4.86																																																										
safety against slipping due to FQ		SG=Fkmin/FkQreq	525.72																																																												
thread strip safety at Rp		m/m min.	1.27																																																												
thread strip safety at FM,max+FSA		tau Rp / tau B,M	3.67																																																												
F A max	N	6.86																																																													
F A min	N	0																																																													
F Q	N	3																																																													
F kreq	N	3.158																																																													
F k min	N	1660																																																													
F M,Re	N	6380																																																													
F M,max	N	3333																																																													
F Mmax,req	N	19.29																																																													
F Mmin,req	N	9.646																																																													
f z	mm	0																																																													
F z	N	0																																																													
F V min,req	N	9.646																																																													
F V min	N	1667																																																													
F V max	N	3333																																																													
F S A,max	N	0.372																																																													
F P A,max	N	6.488																																																													
F R m	N	10684																																																													
F Rp	N	9657																																																													

7713 Project
Bolt Analysis

Figure D.1: Results sheet for bolt analysis [28].

APPENDIX-E

MEASUREMENT UNCERTAINTY OF THE DATA

Measurement uncertainty is a function of the measurement system. It is necessary to completely define the measurement system before proceeding with an uncertainty analysis. After that definition, error sources may be treated as either precision or bias.

Sources of precision error or random error add a component to the result, whenever a measurement is made. This component is unknown but it changes in a random fashion with repeated measurements. Therefore, the error component added to the next measurement is uncorrelated to what was added to the first one. Each measurement has a random error component which is uncorrelated.

E.1 Gaussian or Normal Distributions

Precision or random error components are drawn from Gaussian or Normal distributions. Hence, error comes from the distribution expressed in the following formula [31]:

$$F(X) = \frac{1}{\sigma\sqrt{2\pi}} e^{-\frac{(X-\mu)^2}{2\sigma^2}} \quad (\text{E.1})$$

where,

μ : the population average (\bar{x} for the best estimates), mean value

σ : the population standard deviation,

X : a population value,

$F(X)$: the frequency with which the value X occurs,

e: the base of natural logarithm.

Population standard deviation in the above equation is defined in the following equation [31]:

$$\sigma = \lim_{n \rightarrow \infty} \left[\left(\frac{\sum (X_i - \mu)^2}{n} \right)^{1/2} \right] \quad (\text{E.2})$$

in which,

X_i : i^{th} data point extracted from the population,

n: number of data points in the population.

The representations of σ and μ can be seen in a Gaussian-Normal distribution plot and Gaussian-Normal histogram shown in Figure E.1.

Figure E.2 shows the time data of a gage reading for each accelerated test scenario. Gaussian-Normal histograms of the corresponding strain data are given in Figure E.3 for one repetition of the life cycle.

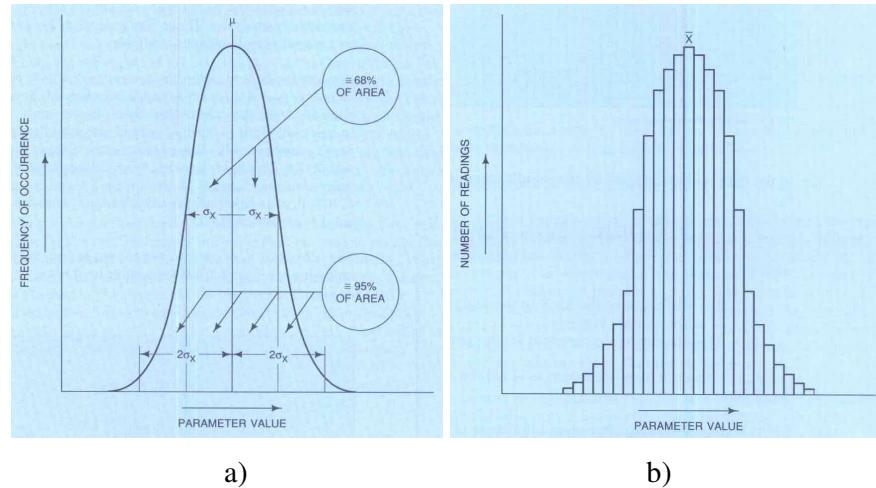


Figure E.1: a) Gaussian-Normal distribution, b) Gaussian-Normal histogram [31].

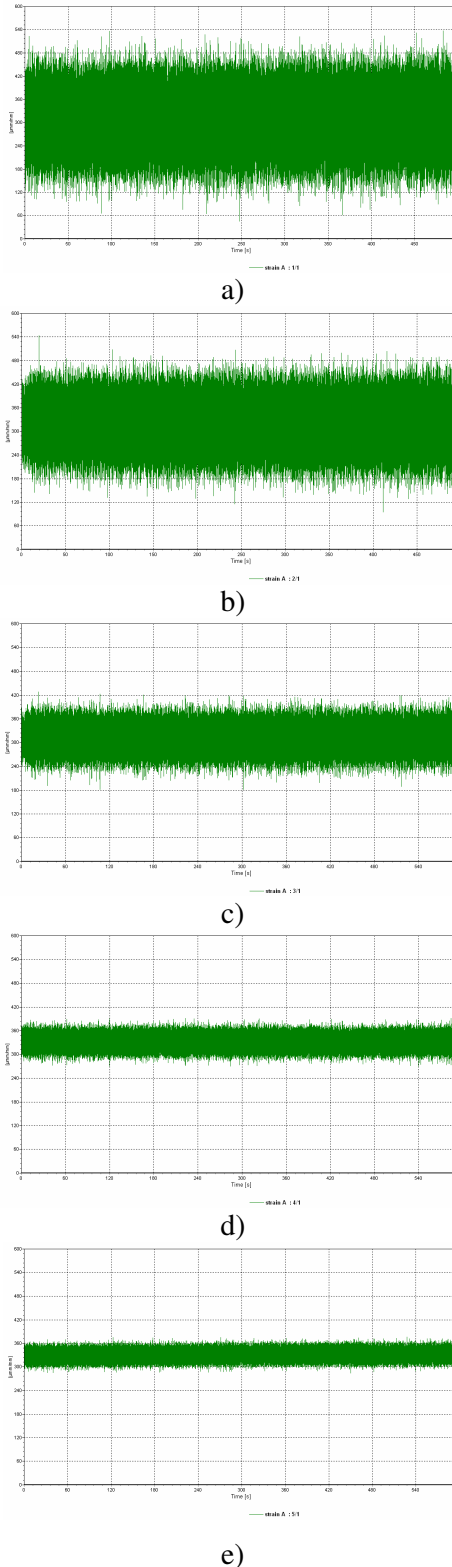


Figure E.2: Time data of strain values for one repetition, strain vs. time, a) 1 hour, b) 4 hours, c) 100 hours, d) 3000 hours, e) 12000 hours accelerated tests.

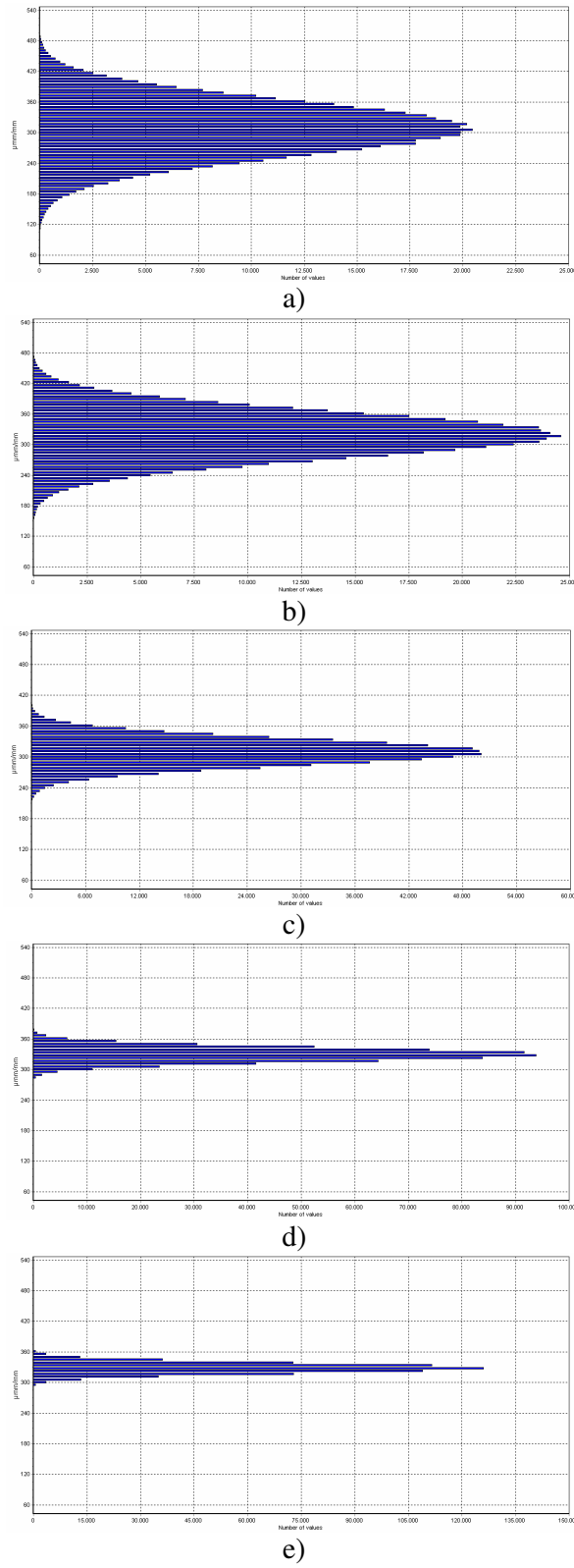


Figure E.3: Gaussian-Normal histograms for one repetition, a) 1 hour, b) 4 hours, c) 100 hours, d) 3000 hours, e) 12000 hours accelerated tests.

Standard deviation calculation for the whole flight test is not appropriate due to high testing costs for test repetition. Therefore, following error estimations are done by considering a single mission. Transverse (Y axis) vibration signal obtained during operational flight tests is analyzed by taking “level flight” mission portion only (Figure E.4). Gaussian-Normal histogram of the data is shown in Figure E.5. Standard deviation of the acceleration data is found by using Esam [24] software. As a result, from Equation.E.2 and by using Esam software $\sigma = 7.56g$.

ICP type accelerometer data has no mean value. Therefore, RMS and standard deviation values are equal. Due to the nature of the test, standard deviation result is not considered as test error.

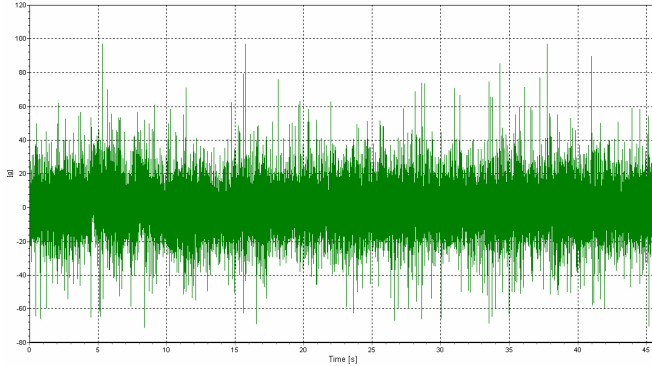


Figure E.4: Acceleration data in transverse (Y) direction for the selected event.

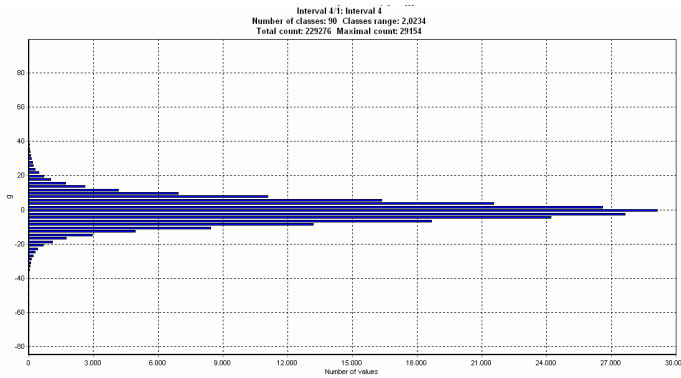


Figure E.5: Gaussian-Normal histogram for the data for the selected event.

E.2. Random Error Estimation

The expected standard deviation of many averages derived from an infinite population of a continuous, Gaussian random variable may be estimated as follows [31],

$$\sigma_{\bar{X}} = \frac{\sigma_x}{\sqrt{N}} \quad (\text{E.3})$$

where,

$\sigma_{\bar{X}}$: Standard deviation of the average, (E_{random})

σ_x : Standard deviation

N: Number of sub-records

Random error associated with the spectral processes in this study can be determined by the below normalized equation:

$$E_{\text{random}} = \sqrt{\frac{1}{N}} \quad (\text{E.4})$$

As a random error parameter, block size of 4096 is used for the spectral processes for a total test time of 78.6 seconds in this study. This results in N=96.

$$E_{\text{random}} = \sqrt{\frac{1}{96}} = 0.102 \text{ or } E_{\text{random}} = 10.2\%$$

E.3. Systematic or Bias Error Estimation

Another important error type is bias error. Bias error is kept constant during the experiment. It affects every measurement of the physical quantity by equal amount. Bias error is not observable in the test data. The reason is the assumption of the experimenter that it is thought that center has been hit by the average of the measurements. Therefore, systematic error is the offset value of the data.

For a high quality measurement, both random and bias errors should be low. Bias error is defined by the following equation [31]:

$$b(G_{ave}(f)) \approx \frac{B_{effective}^2}{24} \cdot \frac{d^2}{df^2} G_{ave}(f) \quad (E.5)$$

where,

$b(x)$: Biased estimate of variable x

$G_{ave}(f)$: Average power spectral density

$b(G_{ave}(f))$: Bias error

$B_{effective}$: Effective bandwidth

For random signal data processes, Equation E.5 is approximated as below,

$$E_{bias} = \frac{1}{3} \left(\frac{B_{effective}}{B_{halfpower}} \right)^2 \quad (E.6)$$

where,

$B_{halfpower}$: Half-power bandwidth

$$\frac{\sigma}{m} = \frac{1}{\sqrt{B_{effective} T_{sub}}} \quad (E.7)$$

in which,

$m=\mu$: mean value

ICP type sensors have no mean value in the measurements. For an accuracy figure (standard deviation/mean value) of unity, that is the lowest accuracy value,

$$B_{effective} = \frac{1}{T_{sub}} \quad (E.8)$$

in which,

$$T_{total} = T_{sub} \cdot N \quad (E.9)$$

T_{sub} : Resolution time

T_{total} : Total record time

Therefore, for a total of 78.6 seconds record with number of block size 4096, effective bandwidth is calculated to be $B_{effective} = 1.22$.

On the other hand, half power bandwidth is defined to be the frequency range between the frequencies at which the PSD value corresponds to half of the maximum value at the resonance frequency. This case is illustrated in Figure E.6, where the transverse axis acceleration data PSD is given.

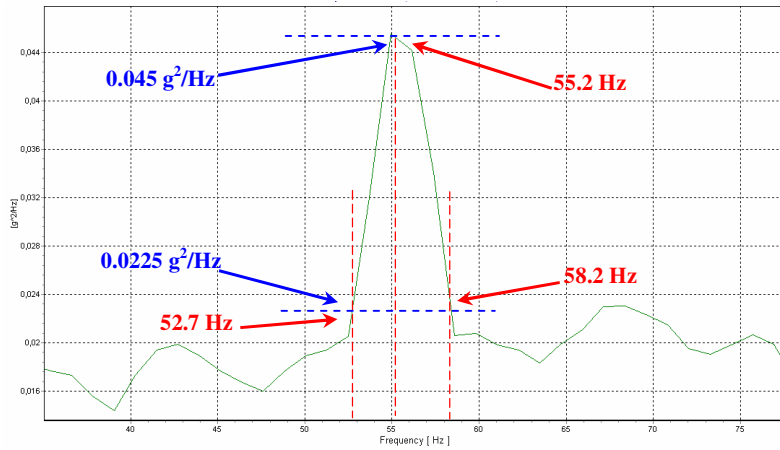


Figure E.6: Schematic determination of half power bandwidth.

Therefore,

$$B_{halfpower} = 58.2 - 52.7 = 5.5$$

Coming back to Equation E.4 and substituting the necessary values,

$$E_{bias} = 0.0164 \text{ or } E_{bias} = 1.64\%$$

According to the error analysis results, total test duration (related to random error) and block size used for spectral processes (related to bias error) are said to be satisfactorily used in this study.

APPENDIX-F

NUMERICAL PSD ANALYSIS OF THE ASSEMBLY

Numerical PSD analysis of the MWS-cowling assembly is performed for determining the deformation behavior of the assembly. Strain data collected in axis by axis vibration tests will be handled according to the result of this numerical PSD analysis result. Therefore, outcome of this study determines the correctness of strain superposition at the analyzed rosette location.

Numerical PSD analysis requires modal analysis solution, just like harmonic analysis. Structural dynamics behavior of the assembly is determined by modal analysis and PSDs are used as loading. Finite element model of the assembly in ANSYS [26] is used for this analysis.

PSD graphs obtained by the operational flight tests are used as loading in numerical analysis. Single PSD analysis is performed for each axis individually. A sample PSD loading plot, defined in ANSYS, is given in Figure F.1.

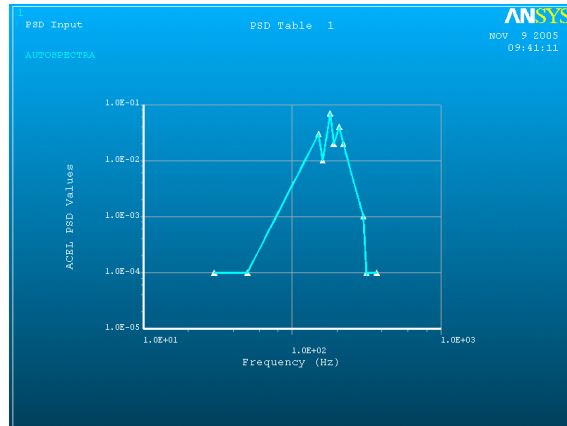


Figure F.1: PSD loading graph in ANSYS [26].

Later on, three dimensional (3D) PSD analysis is performed, meaning that PSD at each axis and cross PSDs are applied simultaneously. Directions of PSD application on the finite element model is given in Figure F.2.

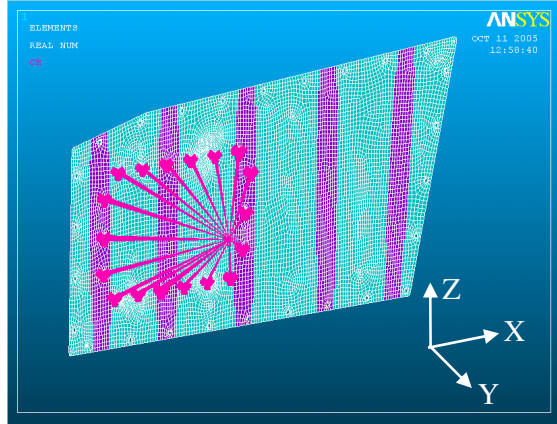


Figure F.2: PSD directions on the numerical model.

Among the three strain rosettes placed on the cowling for strain recording, the one next to the MWS sensor is selected to be analyzed (Figure F.3). The reasons for selecting that strain rosette can be listed as follows:

- It is placed next to the sensor and first few modes of the assembly excite that location,
- It is not located at the boundaries. Therefore, it will reflect the dynamic behaviors of the cowling.

Therefore, a node on the finite element model is selected at the location where the strain rosette is placed. In Figure F.4, selected node at the rosette functioning region is shown. This node has a distance of 9.4 mm to the edge of the nearest hole, as it is measured on the physical prototype. Node number of the selected node is determined as 36921.

Therefore, strain values at node number 36921 should be noted after each PSD analysis, in order to discuss the dynamic characteristics of the location.

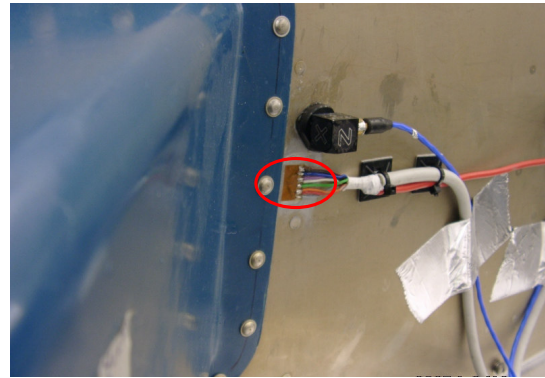


Figure F.3: Strain rosette location to be analyzed.

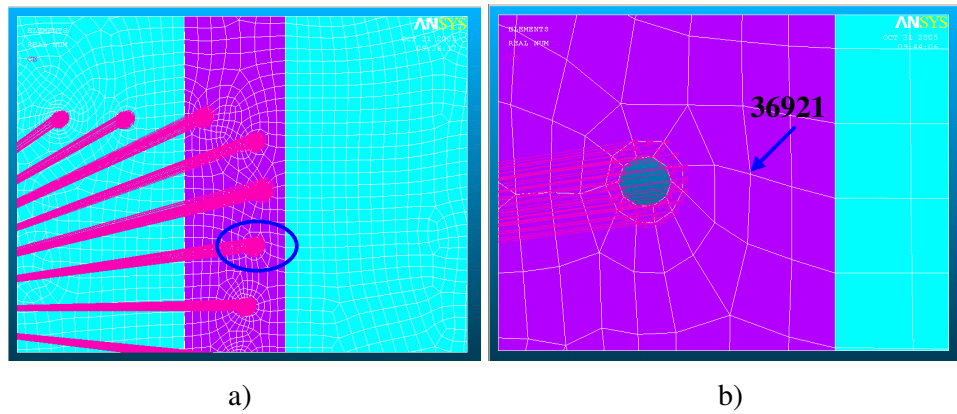


Figure F.4: Node number 36921 to be used in analysis, a) Wide view, b) Closer view.

PSD analysis of the assembly is performed in each axis and in a multiaxial manner. Figure F.5 to Figure F.7 show the strain component values obtained by applying PSDs at each axis individually for node number 36921. On the other hand, Figure F.8 gives the strain component values for 3D simultaneous PSD analysis. It should be noted that there are 2 nodes with the same node number. This is due to shell element definition. One of these nodes corresponds to the top surface of the cowling, and the other one corresponds to the bottom surface.

In order to distinguish these nodes, first one will be denoted as 36921-1 and the second one will be denoted as 36921-2.

NODE	EPTOX	EPTOY	EPTOZ
36920	0.66877E-05	0.96057E-05	0.39862E-05
36920	0.69938E-05	0.10234E-04	0.39912E-05
36921	0.25375E-05	0.10258E-05	0.46689E-05
36921	0.25350E-05	0.16285E-05	0.40315E-05
36922	0.16786E-04	0.23412E-04	0.10672E-04
36922	0.17008E-04	0.25160E-04	0.93752E-05
36923	0.93977E-05	0.25549E-04	0.80990E-05

Figure F.5: Strain components for PSD analysis in X-direction.

NODE	EPTOX	EPTOY	EPTOZ
36920	0.16732E-04	0.23794E-04	0.10495E-04
36920	0.17836E-04	0.25940E-04	0.10828E-04
36921	0.87324E-05	0.30210E-05	0.14246E-04
36921	0.80397E-05	0.46610E-05	0.11309E-04
36922	0.50503E-04	0.69133E-04	0.33487E-04
36922	0.50391E-04	0.73578E-04	0.28766E-04
36923	0.28233E-04	0.74956E-04	0.22519E-04

Figure F.6: Strain components for PSD analysis in Y-direction.

NODE	EPTOX	EPTOY	EPTOZ
36920	0.17630E-05	0.24395E-05	0.12475E-05
36920	0.18484E-05	0.26097E-05	0.13015E-05
36921	0.62142E-06	0.20499E-06	0.11546E-05
36921	0.61227E-06	0.33175E-06	0.10605E-05
36922	0.85922E-05	0.11846E-04	0.56011E-05
36922	0.83807E-05	0.12108E-04	0.49108E-05
36923	0.48298E-05	0.12672E-04	0.36656E-05

Figure F.7: Strain components for PSD analysis in Z-direction.

NODE	EPTOX	EPTOY	EPTOZ
36920	0.20624E-04	0.29539E-04	0.12819E-04
36920	0.21804E-04	0.31880E-04	0.13264E-04
36921	0.11047E-04	0.38293E-05	0.18346E-04
36921	0.10289E-04	0.59813E-05	0.14930E-04
36922	0.73154E-04	0.10091E-03	0.47673E-04
36922	0.72943E-04	0.10669E-03	0.41435E-04
36923	0.40971E-04	0.10928E-03	0.33114E-04

Figure F.8: Strain components for multiaxial (3D) PSD analysis.

The meaning of adding the single axis strain components is investigated. In order to see how correct it is to add these components, comparison study is performed with the multiaxial PSD analysis results. The analysis is done for strain components of node number 36921.

Strain analysis and relative error calculations for node number 36921 based on single axis and multiaxial PSD analyses are given in Table F.1 and Table F.2.

Table F.1: Strain addition analysis for node number 36921-1.

node	strain x	strain y	strain z	
<i>36921-1</i>	2,53E-06	1,02E-06	4,66E-06	x-axis
	8,73E-06	3,02E-06	1,42E-05	y-axis
	6,21E-07	2,04E-07	1,15E-06	z-axis
	1,18E-05	4,24E-06	2,00E-05	3D (summation)
	1,10E-05	3,82E-06	1,83E-05	3D (simultaneous)
	8,1	11,0	9,2	% error

Table F.2: Strain addition analysis for node number 36921-2.

node	strain x	strain y	strain z	
<i>36921-2</i>	2,53E-06	1,62E-06	4,03E-06	x-axis
	8,03E-06	4,66E-06	1,13E-05	y-axis
	6,12E-07	3,31E-07	1,06E-06	z-axis
	1,11E-05	6,60E-06	1,64E-05	3D (summation)
	1,02E-05	5,98E-06	1,49E-05	3D (simultaneous)
	9,0	10,5	9,8	% error

It is seen that addition of strain components (strain superposition) is acceptable within a range of approximately 10% error. However, it should be noted that this analysis is valid for this specific structure. The result is an outcome of the assembly's dynamic characteristics under operational PSD loading.

In fact, the outcome of this study is quite satisfactory for the assembly. 10% error for the strain results can be considered to be acceptable.

APPENDIX-G

RIVETING SIMULATION FOR RESIDUAL STRESSES ON THE COWLING

Effect of mean and/or residual stresses is very significant in fatigue and stress evaluations. Assembly stresses are one of the major sources of residual stresses. Rivets are the most commonly used connection elements in aerospace. Riveting is performed by using an air gun. Physical air gun and its application are shown in Figure G.1.



Figure G.1: a) Air gun equipment, b) Riveting application [18].

In the MWS-cowling assembly, there exist two riveted joints in the region of analysis near the rosette. One of them is countersunk head rivet and the other one is universal head rivet. These riveted joints are shown in Figure G.2.

MSC Marc [33] software is used as a finite element analysis tool for riveting simulation. The software is selected due to its strength in nonlinear analyses, such as metal forming processes.

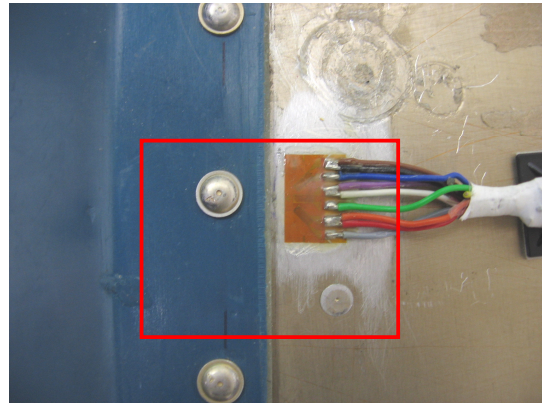


Figure G.2: Riveted joints near the rosette.

Riveting simulations are usually performed by using two dimensional axis symmetric (2D) models. However, this is only possible when a single rivet is to be squeezed. In such cases, finite element model is prepared as it is given in Figure G.3.

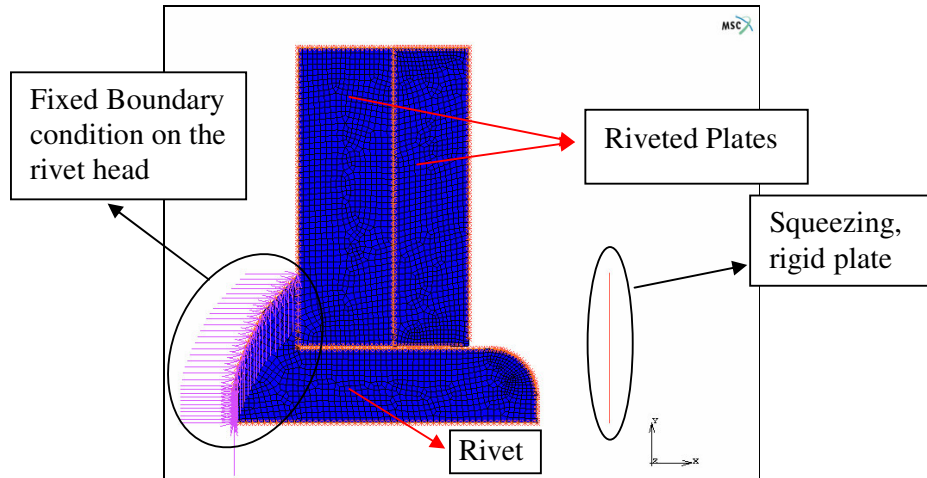


Figure G.3: 2D riveting simulation model.

In this analysis, a portion of the cowling-composite-stiffener-rivets connection region is modeled. This region is shown by a red rectangle in Figure G.2. Since there are two rivets to be included in the simulation, three dimensional (3D) finite

element model of this portion is prepared by using 15130 elements. This model is given in Figure G.4.

The element size of the rivet models is very critical for the analyses. Since riveting is a highly nonlinear process, large distortions may occur in the elements. As a result, solution may not converge. Among the 15130 elements in the finite element model, 3420 elements are used for the rivet that connects composite to the cowling, and 1746 elements are used for the rivet that connects stiffener to the cowling. Material of the rivets is 2117-T4 aluminum. The models for two rivets are shown in Figure G.5.

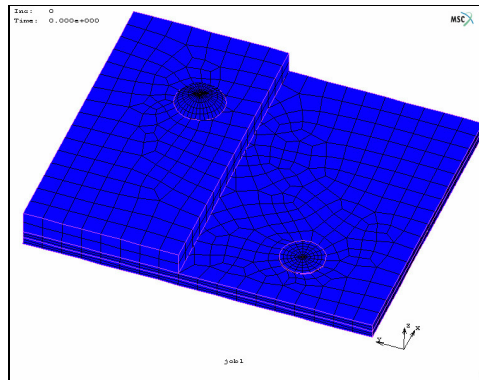


Figure G.4: Finite element model prepared in MSC Marc [33].

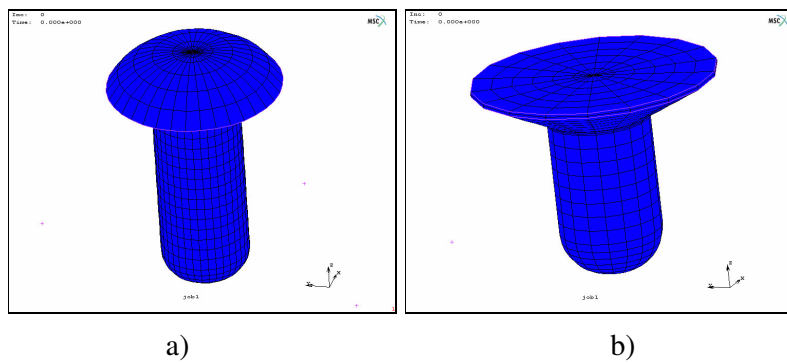


Figure G.5: Models of rivets, a) Universal head rivet, b) Countersunk head rivet.

Boundary conditions are defined on the finite element model. Rivet heads are held fixed. In addition, edges of the modeled portion are fixed as well.

Composite portion of the assembly is 45° glass fiber composite. The mechanical properties of the composite have been determined by an earlier ASELSAN study. Therefore, the result of the study is directly used by referencing the related document [34].

Mechanical properties of the composite are taken as below.

$$E_x = 20 \text{ GPa}, E_y = 19 \text{ GPa}, E_z = 1 \text{ GPa}$$

$$G_{xy} = 8.6 \text{ GPa}, G_{xz} = 8.6 \text{ GPa}, G_{yz} = 1 \text{ GPa}$$

$$\nu_{xy} = \nu_{xz} = \nu_{yz} = 0.13$$

By using the above material data, it is assumed that composite behaves like it is given in Figure G.6. This is an appropriate approximation for this study. The area of interest is not the composite region. The stress value will be obtained on the aluminum cowling.

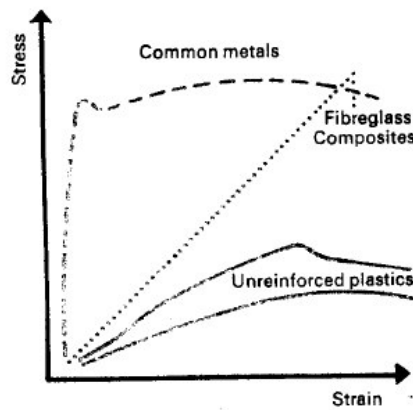


Figure G.6: Stress-strain curve estimation of fiber glass composites [35].

Isotropic material properties for 2024 - T3 aluminum is used in the analysis [36].

$$E = 73.1 \text{ GPa}, \nu = 0.33, \sigma_{yield} = 345 \text{ MPa}, \sigma_{UTS} = 483 \text{ MPa}$$

Two rigid punches are created for activating the riveting process. Firstly, countersunk head rivet that connects stiffener to the cowling is squeezed. As first punch moves away from the rivet end, second punch starts squeezing the universal head rivet that connects composite to the cowling. A relatively slow penetration velocity, 0.2 mm/s, is defined due to avoid diverging solution.

Punches and their locations under undeformed rivets are shown in Figure G.7.

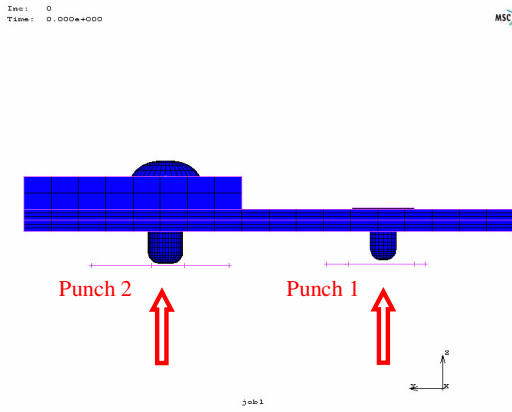


Figure G.7: Punches and their order of penetration.

Analysis options are set as below:

- Elastic-plastic behavior is defined as the deformation characteristics of the components,
- Large displacement (large strain) option is taken into consideration,
- Implicit solution type is selected, since stress results will be used.

Friction coefficients for metal-metal and composite-metal contact are taken as 0.75 and 0.45, respectively [37].

Total time duration for the analysis is set to 24 seconds. This is completed in 200 sub steps, meaning that 0.12 seconds is defined as the constant time step. Actual analysis is completed in 8 hours.

After completing the run, maximum principal stress in the cowling is the main point of interest for the study. This is done for determining the maximum possible stress value at the rosette location. It is going to be used for modifying the raw strain data to have the determined residual stress in the data.

Maximum principal stress value distribution of the analyzed model is shown in Figure G.8 and Figure G.9.

After carefully inspecting the area of rosette location, it is seen that tensile stress range of 0-20 MPa is present. The distance of the rosette's effective point to the edge of the nearest hole is determined on the physical prototype. The distance is used for locating the useful node of maximum principal stress determination.

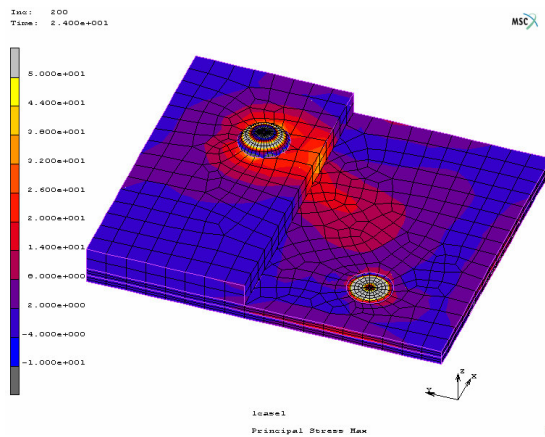


Figure G.8: Maximum principal stress distribution- top view.

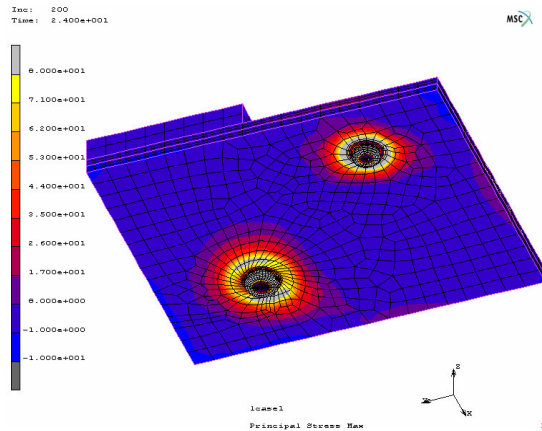


Figure G.9: Maximum principal stress distribution- bottom view.

As a result of the analysis, maximum principal stress of 8.8 MPa is obtained at the rosette placement location. It is used in Chapter 7 for modifying the raw strain data in order to include the residual stresses due to riveting process.

In addition to the previous stress distribution graphs, residual stresses on the rivets are also given in Figure G.10. This is important to identify the regions under compression and tension. Both rivets have similar stress distributions on them. It is seen that maximum compressive stress of about 100 MPa and maximum tensile stress of about 200 MPa is present on both of the rivets.

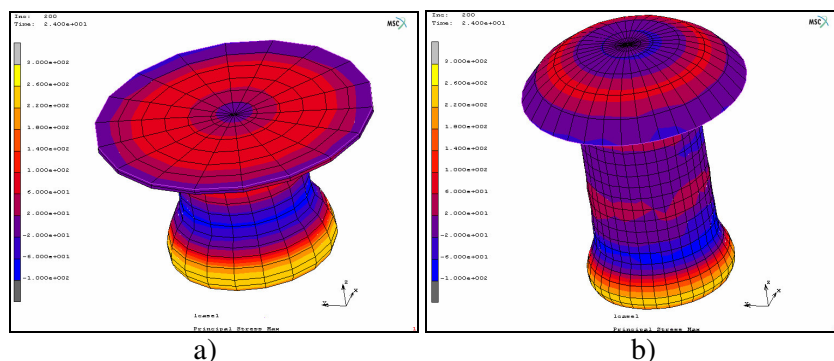


Figure G.10: Maximum principal stress distribution on the rivets, a) Countersunk head rivet, b) Universal head rivet.

APPENDIX-H

STRAIN ROSETTE ANALYSIS THEORY

The ability to determine strains and stresses accurately have been becoming more and more important, in order to accelerate the calculation and design process without being unreliable. This need led to the evolution of new calculation methods to be used in stress analysis, and to the development of new instruments for determining strain experimentally.

Earlier methods of strain measurement employed direct mechanical measurement on the part, often supplemented by optical amplification to overcome the difficulty of slight changes in length. The strain gage was developed in the late thirties by two researchers, Simmons and Ruge, in the USA. They developed a strain gage consisting of a length of wire glued to the test object so that changes in length on the surface are transferred to the wire [38]. The modern strain gage works in exactly the same way.

Typical well known applications for strain gages include experimental strain and stress measurement on aircrafts, boats, cars, pressurized containers, bridges, dams, buildings, etc. An application of strain gages in defense industry is shown in Figure H.1.

Strain gages with two or three elements are called Rosettes. Each gage on a rosette is placed at a certain angle to the others. As mentioned before, three element strain gages (rosettes) are widely used. Since three element rosettes are used in this study, brief formulae definitions of the kind will be covered in this section. A general representation of three element strain gages is shown in Figure H.2.



Figure H.1: Strain gage application on a missile launcher system [7].

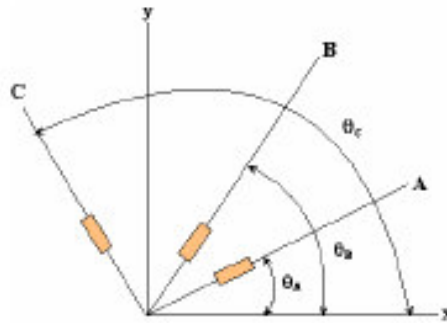


Figure H.2: General representation of three element strain gages.

For such a gage arrangement as shown in Figure H.2, each gage's individual reading can be directly written as:

$$\varepsilon_A = \varepsilon_{xx} \cdot \cos^2 \theta_A + \varepsilon_{yy} \cdot \sin^2 \theta_A + \gamma_{xy} \cdot \cos \theta_A \cdot \sin \theta_A \quad (\text{H.1})$$

$$\varepsilon_B = \varepsilon_{xx} \cdot \cos^2 \theta_B + \varepsilon_{yy} \cdot \sin^2 \theta_B + \gamma_{xy} \cdot \cos \theta_B \cdot \sin \theta_B \quad (\text{H.2})$$

$$\varepsilon_C = \varepsilon_{xx} \cdot \cos^2 \theta_C + \varepsilon_{yy} \cdot \sin^2 \theta_C + \gamma_{xy} \cdot \cos \theta_C \cdot \sin \theta_C \quad (\text{H.3})$$

The components of strains, ε_{xx} , ε_{yy} and γ_{xy} , can be easily determined by using the above equations. Furthermore, the principal strains and their directions can be calculated by employing:

$$\varepsilon_{1,2} = \frac{\varepsilon_{xx} + \varepsilon_{yy}}{2} \pm \frac{1}{2} \cdot \sqrt{(\varepsilon_{xx} + \varepsilon_{yy})^2 + \gamma_{xy}^2} \quad (\text{H.4})$$

$$\tan 2\theta = \frac{\gamma_{xy}}{\varepsilon_{xx} - \varepsilon_{yy}} \quad (\text{H.5})$$

If the material is homogenous and isotropic, Hooke's Law can be used with the above equations to calculate the principal stresses, by defining elastic modulus (E) and the Poisson's ratio (ν).

$$\sigma_1 = \frac{E}{1-\nu^2} \cdot (\varepsilon_1 + \nu \cdot \varepsilon_2) \quad (\text{H.6})$$

$$\sigma_2 = \frac{E}{1-\nu^2} \cdot (\varepsilon_2 + \nu \cdot \varepsilon_1) \quad (\text{H.7})$$

For the most common three element strain gages, rectangular rosette and delta rosette, θ values are used as:

Rectangular rosette $\rightarrow \theta_A = 0^\circ, \theta_B = 45^\circ, \theta_C = 90^\circ$

Delta rosette $\rightarrow \theta_A = 0^\circ, \theta_B = 120^\circ, \theta_C = 240^\circ$

APPENDIX-I

SKETCH OF THE ANALYZED LOCATIONS

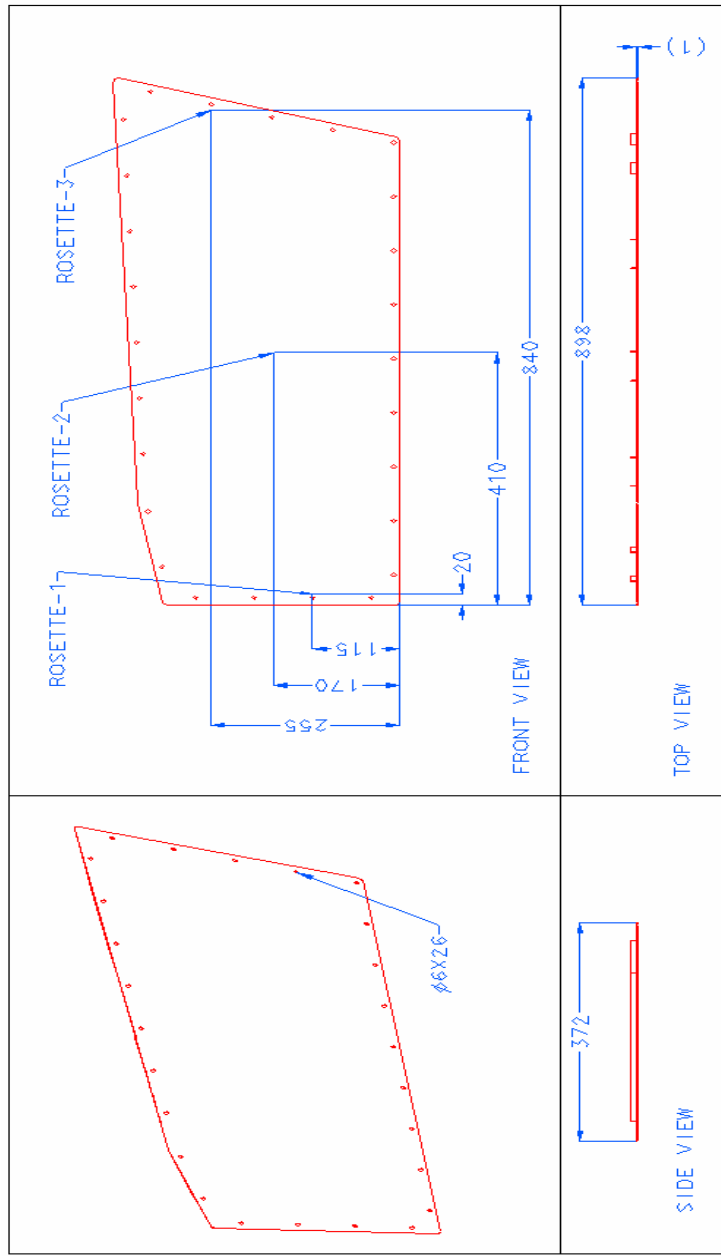


Figure I.1: Sketch of the cowling and the analyzed locations on the cowling (all dimensions are in millimeters).

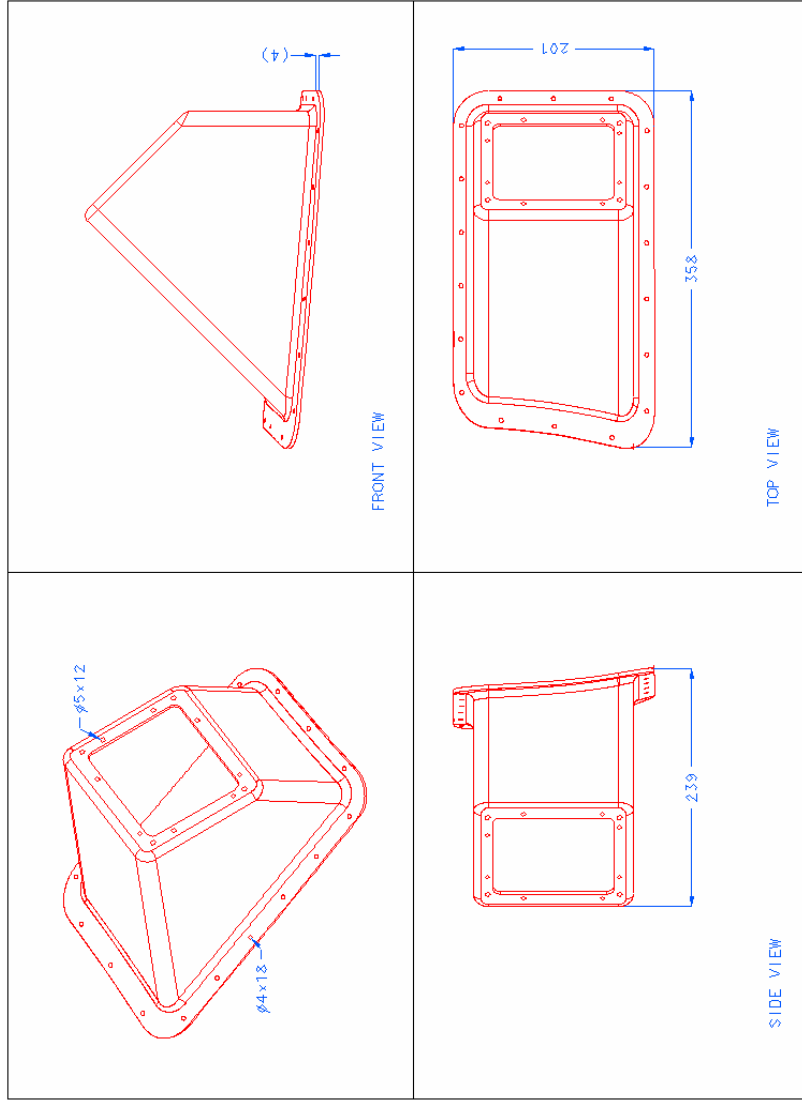


Figure I.2: Sketch of the composite MW S bracket (all dimensions are in millimeters).